Chemical Geology
March 2023, Volume 621, Pages 121278 (17p.)
https://doi.org/10.1016/j.chemgeo.2022.121278
https://archimer.ifremer.fr/doc/00813/92517/

2H-2H clumping in molecular hydrogen method and preliminary results

Mangenot Xavier [1, 2, 6, *], Xie Hao [1], Crémière Antoine [1], Giunta Thomas [3], Lilley Marvin [4], Sissmann Olivier [5], Orphan Victoria [1], Schimmelmann Arndt [7], Gaucher Eric [2], Girard Jean-Pierre [2], Eiler John [1]

[1] Department of Geological and Planetary Sciences, Caltech, Pasadena, CA, USA
[2] TotalEnergies, EP/R&D, Pau, France
[3] IFREMER, Unité des Géosciences Marines, Plouzané, France
[4] University of Washington School of Oceanography, Seattle, WA, USA
[5] IFP Energies Nouvelles, Rueil-Malmaison, France
[6] Department of Geological Sciences, University of California, Santa Barbara, CA, USA
[7] Department of Geological Sciences, Indiana University, Bloomington, IN, USA

* Corresponding author : Xavier Mangenot, email address : xmang@caltech.edu

Abstract :

We present a method for measuring the clumped isotope composition of molecular hydrogen (H2) using a high-resolution mass spectrometer, the Thermo 253 Ultra, improved to address subtle artifacts arising from instrument baselines and non-linear responses. We also present methods for purification and concentration of H2 from natural and experimental samples, tailored to this measurement. We document the accuracy of the method through comparison to established methods for the determination of δD values, and through measurements of H2 gases of widely varying D content that were driven to isotopic equilibrium with respect to their distributions of isotopologues by heating in the presence of a catalyst. Experimental reproducibility of δD and ΔDD values over months averages ±0.5 and ± 6.9 ‰, respectively (1σ) — both small fractions of common natural variations. We explore methods of gas purification and handling, and show that preferred methods result in low (0–4 ‰) changes in δD and undetectable changes in ΔDD. Our methods and data processing procedures were further tested by comparing measurements of mixtures of H2 gases that varied widely in δD and ΔDD with a model describing proportions of isotopologues in such mixtures. Application of these methods to H2 that is residual to laboratory consumption by cultured methanogens shows that metabolic 'back reaction' (metabolic production of H2 from water-derived protons during net H2 consumption) is responsible for driving the ΔDD value of residual H2 toward equilibrium at environmental temperatures. Finally, we report the first measurements of the clumped isotope composition of molecular hydrogen in natural geological samples collected from high and low temperature submarine hydrothermal vents (Lost city, Rainbow, Ashadze) and an intracontinental natural reservoir in Mali; initial findings suggest that ΔDD of H2 generally records temperatures of fluid venting or long-term storage, even in cases where the δD of H2 has not equilibrated with water at those temperatures. This study establishes the first clumped isotope systematics of molecular hydrogen based on both experimental and natural samples, including key processes in the biogeochemical cycle of H2.

Highlights

► First clumped isotope measurements on natural H_2 samples ► Method improved to correct for instrument baselines and non-linearity issues. ► ΔDD generally records temperatures of fluid venting or long-term storage. ► Cultured hydrogenotrophic methanogens drive the ΔDD value of residual H_2 toward equilibrium at environmental temperatures.

Keywords : Molecular hydrogen, Stable isotope, Clumped isotope, Hydrogenotrophic methanogenesis, Geological H2

1. Introduction

Molecular hydrogen (H_2) is a small and simple but essential chemical compound. It is the most abundant molecule in the universe (Palla *et al.* 1983), strongly increases the ability of interstellar matter

to radiate heat (i.e., relative to the abundant pool of atomic H), and therefore has an outsized impact on the formation of stellar systems (Shull and Beckwith, 1982). H_2 is the dominant constituent of circumstellar gas disks and strongly influences early disk chemistry, including synthesis of prebiotic organic compounds. On rocky bodies, H_2 can be produced abiotically through rock-water interaction, as documented on Earth in active hydrothermal systems and aqueously altered rocks across a wide range of continental and submarine settings, including mid-ocean ridges and back-arc spreading centers, ridge flanks, transform faults, fractures zones, subduction zones, passive margins, intracratonic basements and intraplate hotspots (Truche *et al.* 2020; Reeves and Fiebig 2020 and references therein). Molecular hydrogen is also generated by life, either directly through microbial metabolisms (Nandi and Sengupta 1998; Hallenbeck and Benemann 2002) or indirectly by thermogenic decomposition of buried organic matter (Tissot and Welte 1984). Geological and biotic sources of H_2 provide metabolic energy that feeds the microbial biomass in the shallow crust (<120 °C) and near-surface soils and waters (Lin *et al.* 2005; Sherwood Lollar *et al.* 2007). Finally, H_2 is generated industrially from both petroleum processing and water electrolysis, the latter of which provides a means of replacing fossil fuels with clean energy sources and so may contribute to efforts to build a low-carbon-emission economy (Eberle et al. 2009).

The large relative mass difference between the two stable isotopes of hydrogen, ^1H (protium) and ^2H (deuterium) induces strong chemical and physical isotope effects (Urey, 1947) and unusually large differences in D/H ratio among natural sources of terrestrial H_2 (Fig. 1; see Hao *et al.* 2020 for review). However, the D/H ratio of molecular hydrogen, which largely reflects the proportions of the isotopologues HD and HH (see section 2, below), taken alone, offers limited and often non-definitive constraints on its origins. The δ^2H value ($D/H_{sample}/D/H_{reference}$ -1) of H_2 reflects the combined influences of several factors, including the δ^2H of its sources of hydrogen atoms, the mechanisms and temperature of formation (Truche *et al.* 2020), reversibility of the chemical process of its formation (equilibrium vs kinetic isotope fractionation), and various isotope effects that may alter the isotope composition of H_2 after its formation (e.g., diffusion, mixing, dissolution in or outgassing from liquids, consumption by abiotic or microbial reactions, or isotopic exchange with other H-bearing compounds like hydrocarbons or water). This final point is particularly problematic because the isotope exchange rate between H_2 and H_2O ($HH + HDO = HD + HHO$) is relatively fast at geologically relevant conditions and timescales (*e.g.,* at 25 °C, the δD of H_2 reaches equilibrium with that of H_2O in less than 500 days at 22 °C, and less than 14 days at 97 °C; Pester *et al.* 2018); and therefore the δD of H_2 is sensitive to isotope re-equilibration during ascent and cooling of high temperature crustal, magmatic and mantle fluids.

Popa *et al.* 2018 recently established a method for determining the proportion of doubly deuterated molecular hydrogen (D_2, or 'DD'; see section 2) with a precision that is generally adequate for observing temperature-dependant equilibrium DD enrichment compared to a stochastic distribution among all H_2 isotopologues. This work provides a second, independent measure of the isotopic properties of molecular hydrogen and therefore potentially opens a new area of research on H_2 geochemistry. Prior studies of multiply substituted isotopic forms ('clumped' isotope species) of other molecules (CO_2, N_2O, C_2H_6, N_2, O_2 and CH_4) have provided insights into a variety of otherwise challenging geochemical and geobiological problems (Eiler *et al.* 2007; Yeung *et al.* 2012, 2016; Stolper *et al.* 2014; Magyar *et al.* 2016; Young *et al.* 2017; Clog *et al.* 2018, Mangenot et al. 2021). These studies give reason to anticipate that measurements of the clumped isotope composition of H_2 would add important constraints for tracing origins and processes. For example, if H_2 forms in and preserves internal isotopic equilibrium, proportions of DD, HD and HH would allow quantitative and relatively unambiguous determinations of the temperatures of molecular hydrogen formation in geological environments, and thus constrain conditions of relevant processes such as serpentinization, hydrothermal activity or microbial metabolic production (Etiope and Lollar, 2013). If instead, the proportions of isotopologues of molecular hydrogen do not conform to internal equilibrium, or undergo re-equilibration after formation, e.g., by isotope exchange with co-existing water, then its clumped isotope composition could serve as a fingerprint for these processes and complement other methods for characterizing the geochemical properties of H_2-bearing gases.

The initial results presented in Popa *et al.* (2018) prove that clumped isotope analysis of molecular hydrogen through high resolution mass spectrometry works in principle and can quantify apparent

temperatures of internal isotope equilibrium. However, several further steps are required to develop this new geochemical system to the point where its use in applied studies is clear. First, we require independent calibration of the scales of measured δD and δDD values, which may be influenced by several analytical and methodological artifacts. It is known that isotope ratio mass spectrometry can provide non-linear responses in measurements of hydrogen isotope ratios, particularly over the very large ranges in δD recognized for natural molecular hydrogen, and may promote fragmentation and recombination of molecules and ions in the ion source, potentially redistributing isotopes among analysed isotopologues (e.g., see Dennis *et al.* 2010 for examples of such effects in clumped isotope measurements of CO_2). Second, it is not yet clear how accurately and reproducibly molecular hydrogen can be isolated and analyzed for its clumped isotope composition when dealing with environmental samples having complex chemistries. And third, no previous study has documented the clumped isotope systematics of molecular hydrogen from important natural settings or their laboratory equivalents.

In this study, we first evaluate the accuracy of high-resolution isotope ratio mass spectrometry (IRMS) using the Thermo 253 Ultra, including potential non-linearities in scales of measured δD and δDD variations. We did this both by comparing δD values measured by high resolution mass spectrometry to those determined by other well documented methods, and by way of a bracketing experiment (see Huntington *et al.* 2009 in which samples with varying starting δD and δDD values were heated at a known temperature to examine whether all converge to the same ΔDD value (i.e., the clumped isotope anomaly, as defined by Popa *et al.* 2018, as should occur if all gases equilibrate and exhibit no non-linearities in their measured δ_i values. Second, we performed a series of heating experiments from 25–850 °C to see whether ΔDD values have the same temperature dependency as predicted by theory, and to appraise and potentially correct for non-linearities that might systematically expand or compress the scale of measured ΔDD values. This procedure allowed us to establish a correction scheme to convert ΔDD data to a common absolute reference frame (ΔDD_{arf}) based on the theoretical temperature dependence of equilibrium clumping in molecular hydrogen, following the principles previously used to develop an absolute reference frame for the clumped isotope analysis of CO_2 (Dennis *et al.* 2010). We then tested our method and data processing procedure by comparing the theoretical predictions of models describing proportions of isotopologues in mixtures of molecular hydrogen gases that differ markedly in isotopic composition against measurements of laboratory mixtures of gases with varying *δ*D and ΔDD values. We also documented long-term experimental reproducibility of measurements of ΔDD_{arf} of a bottle of pure H_2, showing it can be measured with a long-term reproducibility of ±7 ‰ (1σ) between analytical session months apart. We also develop methods for gas handling on various vacuum apparatus and gas concentration devices, showing a preferred method that does not measurably influence ΔDD composition. Finally, we conducted the first measurement of the clumped isotope composition of molecular hydrogen from natural geological samples — high and low temperature submarine hydrothermal vents (*Lost city, Rainbow, Ashadze*) and a continental geological reservoir in Mali — and from laboratory microbial cultures of hydrogenotrophic methanogens. These data establish the accuracy and precision of clumped isotope measurements of natural samples of molecular hydrogen and document the isotope systematics of key components of the natural biogeochemical cycle of H_2.

2. Theory and Nomenclature

Reviews of the theory and nomenclature of clumped isotope geochemistry are presented in Eiler (2007, 2011, 2013), Wang *et al.* (2004) and Stolper *et al.* 2014; here we further develop these concepts for the case of H_2. In molecular hydrogen, ^1H and ^2H isotopes can combine to form three diatomic isotopologues: ^1H-^1H (unsubstituted, denoted HH here, to distinguish it from the chemical formula for molecular hydrogen generally, H_2), ^1H-^2H (singly substituted, denoted HD) and ^2H-^2H (doubly substituted, denoted DD). If the atoms combine in a purely stochastic way, the fractal abundance of [HH] molecules in natural, D-poor H_2 will be close to 1 ($[HH] = [H]^2$, where [i] of molecules denotes a fraction of all molecules of a compound in question, and [i] of atoms denotes a fraction of all atoms of an element in question); the proportion of [HD] will be close to twice the abundance of the total [D] atoms, as the symmetry number ratio between HH and HD is 2 ($[HD] = 2*[H]*[D]$); and the stochastic fractional abundance of doubly substituted [DD] molecules will be $[DD] = [D]^2$ ($\sim \{[HD]/2\}^2$).

The proportions of isotopologues containing more than one rare, heavy isotope (a "clumped" isotopologue) are often not random (see Eiler, 2007), i.e., they depart from the stochastic distribution. Clumped isotopologues are generally favored under conditions of chemical equilibrium and become more abundant at low temperature. For the reaction:

$$2\ HD = HH + DD \quad \text{(eq. 1)}$$

the right side of the equation, which contains the clumped species DD, is thermodynamically favoured because it has lower total zero-point energy than the left. Hence, for a given bulk isotopic composition (δD), this results in DD being more abundant at equilibrium; this DD enrichment is pronounced at low temperatures and attenuated at high temperatures due to the increasing thermodynamic importance of configurational entropy at higher temperature. HH is similarly enriched, and HD is correspondingly depleted compared to stochastic proportions, but by amounts that are insignificant relative to their random proportions in natural, D-poor H_2. We normalize the enrichment or depletion in DD relative to the stochastic state using the ΔDD value, calculated as follows:

$$\Delta DD = [(^{DD}R/^{DD}R^{*})-1]*1000 \quad \text{(eq. 2)}$$

where $^{DD}R = [D_2]/[H_2]$ and the * denotes the same ratio for a population of H_2 molecules having the same D/H ratio as the sample being reported, but a stochastic distribution of isotopologues. Assuming that the unsubstituted and singly substituted species (HH, HD) are present in in their stochastically predicted proportions (the error caused by this assumption is trivial compared to current analytical precision), eq. 2 can be reformulated as follow:

$$\Delta DD \sim [4*(^{DD}R/^{HD}R^{2})-1]*1000 \quad \text{(eq. 3)}$$

Where $^{DD}R = [D_2]/[HH]$ and $^{HD}R = [HD]/[HH]$.

The ΔDD value for H_2 that has reached equilibrium with respect to eqn. 1 (Gould *et al.* 1934; Rittenberg *et al.* 1934; Urey, 1947) varies from 0 to 243 ‰ between 1000 and 0 ˚C, respectively, with a temperature sensitivity of around 1 ‰ per degree C at 25 °C, and around 0.1 ‰ per degree at 500 °C (Popa *et al.* 2018). Thus, a measurement that precisely constrains the natural abundances of the three isotopologues of H_2 may serve as a geothermometer that records the temperature of H_2 formation or last equilibration. Additionally, non-equilibrium, *i.e.*, irreversible, or kinetically controlled processes may cause distinctive fractionations among isotopologues that lead to clumped isotope compositions (Δ_i values) that differ from those expected for equilibrium at ambient environmental temperatures. In these cases, quantification of ΔDD values of H_2 might contribute to recognizing and quantifying features of kinetic processes, as has been done using clumped isotope characteristics of CO_2, C_2H_6, N_2O, O_2, N_2, CH_4 and methoxy groups (Eiler *et al.* 2004; Yeung *et al.* 2012; Wang *et al.*, 2015; Magyar *et al.* 2016 ; Clog *et al.* 2017; Young *et al.* 2017 ; Labidi *et al.* 2020; Dong *et al.* 2021, Loyd *et al*. 2021).

Figure 1 shows abundances of the H_2 isotopologue, DD (colour fill, keyed to the right-side scale) over most of the range of δD_{VSMOW} measured in geological H_2 samples to date (–850 to –100 ‰, excepting higher values seen in the atmosphere) and the full range in ΔDD values expected for hydrogen equilibrated in common geological conditions. In this compositional space, DD varies in natural abundance between 2 and 25 ppb, as a fraction of all H_2 molecules. As an example, a gas with δD_{VSMOW} of -720 ‰ and ΔDD of 220 ‰ (*e.g.*., low temperature equilibrium) will contain a total of 2.32 ppb of DD, and only 0.41 ppb 'extra' D_2 molecules compared to its stochastic abundance (1.90 ppb). The same calculation for a gas with δD_{VSMOW} of -120 ‰ and ΔDD of 50 ‰ (corresponding to temperatures approaching 500 ˚C) corresponds to 18.7 ppb of DD and around 1 ppb excess compared to the stochastic distribution. The low concentrations expected for DD, combined with the desire of a precision on the order of ‰ to perform geothermometry, make analysis of isotope clumping in molecular hydrogen a substantial technological challenge.

3. Mass spectrometry methods

Mass spectrometric measurements of hydrogen isotopic ratios in H-bearing compounds typically employ molecular H_2 as the analyte gas, and determine the abundance ratios between HH (m/z=2) and HD (m/z=3). An unfortunate consequence of the use of H_2 for these measurements is that the reaction 4 occurs readily in the ion source of the mass spectrometer.

$$H_2^+ + H_2 = H_3^+ + H^* \text{ (eq. 4)}$$

Since H_3^+ (m/z=3.02293) is not mass-resolved from HD^+ (m/z=3.02138) by conventional gas source isotope ratio mass spectrometers (mass resolutions ~200), a correction is required to account for the contribution of H_3^+ to HD^+ (i.e., the H_3 factor; Sessions *et al.* 2001). In materials containing a natural abundance of D, H_3^+ can account for as much as 5-60% of the m/z 3 signal. Similarly, study of DD+ at m/z = 4 must contend with nearly isobaric interference with the H_2D^+ adduct, which is typically ~10-fold more abundant than DD+ (see **Figure 2**). Furthermore, measurements of DD^+ (m/z=4.02765) must avoid contributions from $^4He^+$ (m/z=4.00205). These m/z=4 ion species are not distinguishable using conventional IRMS instruments.

Mass spectrometrically clean analysis of HD and DD isotopologues requires mass resolution sufficient to resolve these isobaric interferences — M/ΔM of at least ~2600, though even higher is likely required to prevent tails of large interfering peaks from dominating the relatively weak signals of HD^+ and, especially, DD^+. Our measurements make use of the Thermo Scientific 253 Ultra (or 'Ultra'), a high-resolution gas source isotope ratio mass spectrometer, housed in the Division of Geological and Planetary Sciences at Caltech. The design and capabilities of a prototype of this instrument are described in Eiler *et al.* 2013 and performance of the production version used for this work is documented in Xie et al., 2020 and Dong et al., 2021. We use the same instrument model, and generally similar methods as used by Popa et al. 2018, though we present modifications and new performance tests of that method. For this work, we use the medium resolution entrance slit that routinely achieves mass resolving powers (MRP; 5 %/95 % definition) between 20,000 and 30,000 on HH (cup L3, 1.10 $^9\Omega$ amplifier) and between 18000 and 20000 on the flat-topped shoulder of HD (cup H1 .10 $^{12}\Omega$ amplifier). DD is measured with a compact discrete dynode ion counter (CDD) that has an 800 μm exit slit (5000-10000 MRP on DD peak).

Figure 2 shows typical peak shapes obtained on HH, HD and DD from different samples measured at the same working pressure (~25 mbar here). With the relatively wide exit slits used here, the HD and DD peaks are mass-resolved from but 'stacked' with the nearby H_3^+ and H_2D^+ peaks, respectively, when a peak scan is performed (i.e., for portions of that scan, both adjacent peaks are fully in the detector, so their signals combine). We therefore select the position where signal will be integrated to lie on the relatively flat shoulder on the low-mass side of the combined peaks, where HD^+ or DD^+ sit, in order to get clean measurements of them. This is an obvious approach and mirrors that in Poppa et al. 2018, but raises the question (unaddressed in prior work) as to whether our chosen measurement position includes ion counts from the tails of H_3^+ or H_2D^+, which might meaningfully impact measurements without being visually obvious in scans such as Figure 2b and c. We examined this question by drastically varying the source pressure, which changes the rates of production of H_3^+ and H_2D^+ and therefore the HD^+/H_3^+ and DD^+/H_2D^+ ratios, and then examined how those changes impacted measurements of the HD^+/HH^+ and DD^+/HH^+ ratios. As shown on Figure S1, we found that both HD^+/HH^+ and DD^+/HH^+ ratios decrease slightly with increasing source pressure and relative intensity of adduct peaks. These negatives trends are opposite in direction to the expected consequences of adduct addition, suggesting we achieved sufficiently high mass resolutions that the diffuse edges of adduct peaks do not significantly influence our measurements. It is not clear to us why the trends of negative slope are observed, but they are similar in amplitude to instrumental biases seen in other IRMS measurements, and could reflect some combination of a pressure dependence of the ion-source mass bias, subtle non-linearity in detector gain, contributions of negative ions produced by a scattered ion beam, and/or background contributions that were not corrected for in the raw data plotted in Figure S1. Whatever is causing this subtle nonlinearity

on the raw ratio, it should be canceled out by sample/standard normalization. We therefore use a conceptually straightforward approach to determining the δD_{WG} and δDD_{WG} values relative to our working gas, by measuring direct HH, HD and DD ion-current ratios without isobaric interreference, as follows:

$$\delta D_{WG} = ((HD/HH_{sample})/ (HD/HH_{reference}) -1)*1000 \text{ (eq. 5)}$$
$$\delta DD_{WG} = ((DD/HH_{sample})/ (DD/HH_{reference}) -1)*1000 \text{ (eq. 6)}$$

The measurement of these three-ion species of interest cannot be performed at the same time because their large relative mass differences result in a dispersion of the three ion beams at the location of the detector array that is larger than the collector plane of the instrument (which corresponds to a dispersion of ~15 % — far less than the factor-2 variation in m/z among our target species). Thus, we use a method based on that presented by Popa *et al.* 2018, in which the different isotopologues are measured sequentially (a method referred as "peak hopping") within an acquisition cycle. In the measurement method presented here, each sequence includes 5 successive acquisition cycles of reference A /sample B (A-B-A-B-A). Each acquisition cycle is composed of (in time order) 10 HH integrations of 0.13 s each, 20 HD integrations of 1 s each and 20 DD integrations of 8 s each. A full measurement includes 5 to 7 repetitions of this sequence, with a pressure adjustment in between each in order to re-balance the HH^+ intensity between sample and standard. At the end of the measurement, we integrate background ions measured at 0.0020 amu to the left side of the HD and DD peaks and then subtract minor, but not zero, background contribution on both (<1000 cps for HD and ~0.02-0.2 cps for DD). Background acquisitions are measured on both standard and samples with ion source pressure adjusted to match the preceding measurement. A complete H_2 sample measurement takes ~3 hours and needs around 80-120 micromoles of H_2 (around 60 % is consumed, and 40% remains in the bellows at the end of the measurement).

4. δ**D calibration.**

To establish the accuracy of our measurements, we compared the δD of two sets of samples measured using both the Ultra and previously established techniques. The first set of samples includes 4 hydrogen gases made by Arndt Schimmelmann at Indiana University by water reduction with uranium at 800 °C, with δD_{VSMOW} ranging from -428 ‰ (SLAP) to +800 ‰. These were stored in flame-sealed quartz tubes prior to analysis at Caltech. The second set includes 8 bottles of isotopically labeled H_2 gases made between 1989 and 2004 by the Oztech Trading Company, with δD_{VSMOW} values ranging between -361 to +101 ‰ and regularly calibrated using international (VSMOW, GISP and SLAP) and in-house standards. One of these Oztech bottles (δD_{VSMOW} = -124 ‰) is used as the internal standard for the Ultra measurements reported here (i.e., the Ultra data are effectively normalized to a common assumed value for this intralaboratory standard). Figure 3 compares our Ultra measurements of these gases to independently determined δD values, all reported on the VSMOW scale. We linearly regressed δD values of samples measured using established techniques (y-axis; Fig. 3) against our measured δD values from the Ultra on the same samples (x-axis). These regressions are error-weighted and incorporate the error in the conventional measurements, which varies from sample to sample. The slope of the line for H_2 gases made by water reduction is 0.99574±0.00463 and the intercept is –0.26±1.69. This best fit line is indistinguishable within 1 standard deviation from a line with a slope of 1 and an intercept at 0. The slope of the line for Oztech H_2-labelled bottles is 0.95191±0.0247 and the intercept is –8.13±4.7, both just at the 2se limit of consistency with a slope of 1 and intercept at 0. Note that the set of isotopically labelled gas bottles is old (30+ years), and we cannot guaranty that their reported δD values remained accurate today; thus we consider the very small departure from the 1:1 line is only marginally significant in a statistical sense, and possibly not meaningful due to the potential for systematic errors in the assumed values. We conclude the bulk isotopic ratios measured by Ultra and conventional techniques on H_2 from water reduction are within error of each other, and that the Ultra can provide satisfactory measurements of the δD of H_2 that can be reported on the same isotopic scale as conventional measurements that have been 'anchored' to the VSMOW-SLAP scale following common conventions for interlaboratory standardization.

5. Defining an absolute reference frame for D-D clumping.

Currently, there are no available H_2 interlaboratory standards with known δDD (or ΔDD) values (and it is not yet clear that ΔDD values are sufficiently stable during storage for the community to create such a material). In this study, we used the heating method presented in the following paragraphs for producing an 'absolute reference frame' for isotope clumping in molecular hydrogen, following an approach previously established for clumped isotope analysis of CO_2, CH_4, N_2O, O_2 and N_2 (Dennis et al., 2010; Stolper et al., 2014; Magyar et al., 2016; Röckmann *et al.* 2016; Yeung *et al.*, 2016, 2017). This practice also allows us to correct for source 'scrambling' (randomization through high-energy fragmentation and recombination reactions), instrument linearity and other analytical and methodological artifacts, and to calibrate temperature-dependent theoretical equilibrium clumping effects with experiments (recognizing that there is an element of circularity in using such data for both purposes). To do so, we used the set of isotopically labelled H_2 bottle gases described above (refer as Oztech gases hereafter) that vary in bulk composition (i.e., δD_{VSMOW} from -361 to 101‰), and equilibrated them to a series of different temperatures by heating them in the presence of Pt catalyst. In the absence of artifacts that correlate with the δD value, we should expect all samples to reach indistinguishable ΔDD values at a given heating temperature. The isotopic compositions of Oztech gases before and after heating are presented in Table S1 and graphically summarized in Fig. 4.

For these experiments we used a U-shape "heating tube" consisting of a heated part made of silica glass and a cold part (including the valve and port) made of borosilicate glass. The tube has small pieces of square Pt catalyst (totalling around 1 gram) at the bottom of the U shape, which promote rapid isotope exchange to drive the reaction given in eq. 1 toward equilibrium. Samples were heated in a box furnace directly adjacent to a calibrated thermocouple in the furnace and connected online to the gas inlet system of the Ultra mass spectrometer. We measured a total of 32 heated gas samples equilibrated at 11 different temperature steps between 25 and 850°C. For any temperature above 100°C, equilibrium was reached in less than 2h (as indicated by the convergence of post-heating ΔDD values for gases that differed markedly in initial ΔDD; see below). At 25°C, the minimum equilibration time is around 20 days.

5.1. Unheated 'Oztech' gas bottles.

Oztech unheated gases display values of δDD that differ remarkably from our intra-laboratory working gas, with δDD_{WG} varying from -520 ‰ to 42000 ‰ (vs. working gas) despite a far more subtle variation in δD values, from -361 ‰ to 101 ‰ (vs. VSMOW, See table S1). The trend defined by these two variables suggests that these reference standards were prepared by mixing natural with highly deuterated H_2, leading to pronounced non-linear 'mixing' effects that are recognized to occur in several clumped isotope systems whenever two, or more, isotopically different endmembers are mixed (e.g., Eiler and Schauble, 2004; Eiler, 2007), and that the gas stored in these cylinders did not undergo intermolecular hydrogen isotope exchange since they were filled (as this process would tend to erase such extreme elevations in ΔDD value). We know these bottles were made by multiple mixing/dilution processes and we initially thought it would be possible to deconvolve the precise stable isotope compositions of the original mixing end members and their relative mixing ratios, based on the measured gas δD and ΔDD compositions and the mathematics describing such non-linear mixing effects. However, the use of multiple dilution steps and different initial endmember through time (1989 to 2004) impedes us from making quantitative interpretations. Importantly, for our purposes, this series of isotopically labelled gases constitute a useful sample set to track our ability to re-equilibrate H_2 gases with respect to their ΔDD values at different temperatures, and thus to establish an absolute reference frame for reporting clumped isotope measurements of molecular hydrogen.

5.2. 'Heated gas lines' and the monitoring of instrument non-linearity

Figure 4 presents data for equilibrated (i.e., heated in the presence of catalyst) gases generated at Caltech between February and September 2021. As shown on panel A of this this Figure, different Oztech gases

having different initial δD and exceptionally different ΔDD values exposed to Pt catalysts at a given temperature and some narrow window of time (4 days or less for temperature range between 77° and 800 °C, over which instrument settings are nearly constant) define linear trends in a plot of post-heating ΔDD vs. post-heating δD (both variables measured vs. a common working reference gas of constant isotopic composition; note only data generated at a single temperature and similar time are fitted with a line). For re-equilibrium at lower temperatures range (*c.f.*, 44° and 22 °C), the heating duration were extended up to 21 days. The relatively flat slopes of these lines document that gases equilibrated at a given temperature very nearly conform to a constant ΔDD_{wg} value, but that statistically significant non-zero slopes fitted to groups of closely related data points indicate a subtle non-linearity in instrument response (i.e., difference between raw measured and true ratios, e.g., due to subtle non-linearities in detector sensitivity and/or subtle variations in background not accounted for in our background measurements and corrections). These linear trends in Figure 4A can be used to empirically define the non-linearity of the mass spectrometer being calibrated (see Huntington *et al.* 2009 for a discussion of non-linearity artifacts in measurements of the Δ_{47} value of CO_2). Specifically, a slope documented in such a figure can be used to define the ΔDD_{wg} value that would have been observed if the sample and standard gases had been identical in δD and therefore relatively similar in ΔDD_{wg} — a condition of near-optimal sample/standard matching where non-linearities in instrument response should be at a minimum. Slopes to fitted lines vary from +0.021 and -0.011 over an 8-month period. These variations are statistically significant and imply that corrections for instrument non-linearity should always be made for measurements of unknown samples, using data for equilibrated heated gas standards measured at the same instrument tuning conditions and close in time (within days). However, we emphasize that the amplitudes of these effects approach the limits of analytical precision and are small relative to natural variations in ΔDD, so these corrections have modest or negligible effects on interpretations of most natural or experimental samples.

5.3. An empirical transfer function relating measured to absolute-reference-frame ΔDD values.

The zero-δD_{wg} intercept of the 'heated gas lines' Figure 4A is defined here as ΔDD_0. Assuming a constant working gas for all measurements on a particular instrument, this value for equilibrated gases is expected to be characteristic of the temperature at which the gas was equilibrated. Because the true ΔDD value of equilibrated H_2 can be independently estimated at each temperature (based on quantum mechanical and statistical thermodynamic theory), we can compare 'true' (theoretically predicted) ΔDD values to ΔDD_0 values for each temperature in Figure 4B. For this study, we have made these determinations for eleven temperatures, documenting a linear trend in Fig. 4B described by the following equation:

$$\Delta DD_{I\_F} = 1.1963\ (\pm 0.0193) * \Delta DD_0 + 233.5\ (\pm 2.3)\ \text{(eq. 7)}.$$

The intercept implies that the intra-laboratory reference gas has an apparent ΔDD composition of +233 ‰ (±2.3), equivalent to apparent temperature of 22±1 °C (lab room temperature is 20 to 24°C). The departure of the slope in Figure 4B from a line of slope 1 reflects the combination of two effects: the differences between 'delta' based scales that have different normalizing reference ratios (i.e., the mathematics behind the 'standard conversion identity' of Craig, 1957), and instrumental artifacts, such as ion source fragmentation and recombination chemistry, which can modify measured scales of variation in clumped isotope indices (e.g., Huntington et al., 2009; Dennis et al., 2010). The first of these factors is the dominant reason the slope in figure 4B departs from 1, and arises because the reference frame for the vertical axis is, effectively, the *stochastic* DD/HH ratio of our working gas whereas that for the horizontal axis is the *true* DD/HH ratio of our working gas. These two differ by a factor of 1.2335, meaning ratios normalized to the true working gas ratio should be compressed in variation by ~23% relative to those same ratios normalized to the stochastic distribution — a good first approximation of the ~20% scale compression that is observed in our 'working gas' reference frame. Note that this, essentially nomenclatural, factor does not appear in a statistically significant way in previously developed clumped isotope indices because their working gases tend to be only modestly

different in relevant ratios from the stochastic prediction (though it is conceivable it could lead to statistically significant systematic errors in $\Delta^{12}CH_2D_2$ of methane). And, this factor does not contribute to the slopes of trends in Figure 4A because the reference ratio for all plotted data is the stochastic DD/HH ratio of the sample itself, i.e., the influence of bulk D abundance on stochastic DD/HH ratios of samples has already been considered in the implied reference frame of Figure 4A.

Figure 4C replots the data from Figure 4B, but using a modified form of measured ΔDD_0 values ($\Delta DD_{0,corr}$), corrected for the scale compression that arises from the 233.5 ‰ enrichment of the DD/HH ratio of the working gas relative to its stochastic distribution. The linear trend in this figure can be fit by the equation:

$$\Delta DD_{ARF} = 1.0223\ (\pm 0.0015) * (1+\Delta DD_0/1000) * (1+233.5/1000). \quad \text{(eq.8)}$$

Where ΔDD_{ARF} is the ΔDD value in the absolute reference frame (i.e., that based on independent estimation of the temperature dependent equilibrium of eq. 1), and the second and third terms in this expression are derived from the standard conversion identity (Craig, 1957). We refer to the empirical factor of 1.0223 ± 0.0015 as the 'non-linearity factor', and its departure from 1 indicates that measured values ΔDD_{WG} are modestly different from actual values by about 2.2±1.5 %, relative, presumably due to unrecognized mass spectrometric artifacts that have been encountered in efforts to construct an analogous 'absolute reference frame' for mass spectrometric measurements of CO_2 (Huntington et al., 2009; Dennis et al., 2010). In principle, the slopes in figures such as Figure 4C could vary with instrument tuning and condition, but data from this study conform to a coherent line over months, suggesting any such variations are smaller than our analytical precision, at least under the conditions and settings used in this study. For the time being, we adopt the parsimonious approach of treating the empirical non-linearity factor as a constant. Because the error on empirical non-linearity factor is only about half of the amplitude of its departure from 1, it might be neglected without incurring substantial systematic errors. However, to ensure the reproducibility of our correction scheme over time, we systematically employed the defined empirical transfer function (ETF, eqn. 8) to convert any measurement of unknown gases into absolute ΔDD_{ARF} values. All the data of this study will hereafter be reported as ΔDD_{ARF} (ARF for Absolute Reference Frame).

As illustrated on Fig 4.D, the translation of this correction scheme to the data for the 32 heated gasses reported here lets us draw a relationship between ΔDD_{ARF} and temperature that is indistinguishable (within measurement errors) in shape and location from the one calculated from quantum mechanical and statistical thermodynamic theory for equilibrated systems between 25 and 1000°C. This result is in some sense an exercise in circular reasoning because of our definition and use of the absolute reference frame (i.e., based on independently known equilibrium constants for eqn. 1). Nevertheless, it provides an effective visual representation of the internal consistency of our data and correction schemes, expressed in a way that can be readily understood in terms of environmental temperatures of equilibrium. We hereafter use the following expression, fit to theoretically predicted temperature-dependent equilibrium constants for eqn. 1, to convert measured ΔDD_{ARF} values into apparent equilibrium temperatures (from Popa et al. 2018):

$$10^6/T^2 = -4E^{-10}*\Delta DD^4 + 2E^{-07}*\Delta DD^3 + 6E^{-05}*\Delta DD^2 + 0.0283\Delta DD + 0.234 \quad \text{(eq. 9)}$$
with T in Kelvin and ΔDD in ‰.

6. Precision and experimental reproducibility

The internal precision associated with each mass spectrometric measurement is calculated based on the standard error of multiple δD and δDD acquisitions (eq. 5 and 6, respectively) measured across a complete set of acquisitions for one sample gas (typically n=10 to 14). These internal errors are typically lower than 0.2 ‰ for δD and around 6 ‰ for δDD and are close to the counting statistical limits for δDD (which averages, by design, 5.4 ‰). Experimental uncertainties associated with analyses of unknown samples may be larger due to random or systematic errors during sample purification, gas

handling and changes in accuracy in the mass spectrometric standardization scheme (i.e., the reference frame presented in section 5), or other unknown factors. Such uncertainties, also known as 'external precision', can be monitored with long term replicate measurements.

We routinely analyzed an 'unknown' sample (i.e., one not used as a standard or to construct our reference frame) taken from a bottle of pure H_2 gas (i.e., without vacuum line manipulation) over a 6-month period (n=15 measurement, Fig. 5). We found that the long-term experimental reproducibility of δD spans a narrow range consistent with a single-measurement error of 0.5 ‰ (1SD), whereas that for ΔDD_{ARF} is consistent with an error of ±6.9 ‰ (1 σ). Both variables are measured with external errors that are only modestly higher than average internal errors of individual measurements, implying there are no major additional errors affecting the measurement and that our intra-laboratory reference frame was stable over a 6-month period. The mean δD_{VSMOW} value of this gas measured with the Ultra (–361.77±0.13 ‰) is within error of the value reported from conventional isotope ratio mass spectrometer measurements (–361.6 ‰). The ΔDD_{ARF} value of this gas is not independently known, but the measured average of 108.6±1.8 ‰ translates into apparent equilibrium temperature of $214_{+4/-5}$ °C.

In addition, we also measured ΔDD values of three high-pressure H_2 cylinders manufactured by AirLiquide and found they all display ΔDD_{ARF} values corresponding to our laboratory room temperature, within errors (Fig. S2). This H_2 was likely produced from high temperature methane steam reforming (at typical furnace temperatures of 900–950 °C), but the ΔDD_{ARF} values seem to have been re-equilibrated at around 20 °C, either during the H_2 purification process at the refinery or latter within the metal cylinders in which they were stored. Our reference gas (an isotopically labeled gas made by Oztech company) shows similar ΔDD/δD composition, perhaps because it originated from such a high-pressurize H_2 cylinder and was likely unmixed with any labeled H_2 gases. It is noteworthy that the low-pressure, small cylinders in which our labeled Oztech gases were stored did not re-equilibrate their ΔDD_{ARF} values over several decades, perhaps implying that storage pressure and/or container material might be factors influencing re-equilibration kinetics. However, we can only speculate about this issue at present but we suggest that controlled studies of re-equilibration during long-term storage should be conducted in the future.

7. Sample preparation, manipulation, and monitoring of stable isotope fractionation

Dual-inlet, gas-source isotope ratio mass spectrometry measurements generally require relatively pure (>99 vol. %) samples. As H_2 is rarely a dominant component of naturally existing gases (e.g., CO_2, N_2, hydrocarbons, or noble gases are generally present as additional components), H_2 needs to be isolated and purified without (or with consistent and correctable) isotopic fractionation. We attempted to do so as follows: The samples are attached to and expanded into a vacuum extraction line (evacuated by a three-stage Hg diffusion pump backed by a two-stage rotary pump) and exposed to a cold trap held at 20 K by a two stage, closed cycle, continuous duty, compressed He refrigeration unit (CTI-Cryogenics, model 8200). The volume of the glass line into which the sample is expanded is around 160 mL and the cold trap's headspace is around 5 mL. We monitor the pressure of the cold trap using a MKS Baratron® capacitance manometer until the pressure stabilizes, indicating that nominally all the N_2, CO_2, O_2, CH_4, and other condensable trace constituents have condensed in the cold trap. This condensing step usually takes less than 2 minutes. The cold trap's headspace is then isolated from the system by closing a valve at the top of that trap (note that the CH_4 or other hydrocarbons retained in the trap can be isolated separately following protocols in Stolper *et al.* 2014, Piasecki et al. 2016, Clog et al. 2018 and Xie et al. 2018, 2020, 2021). Gases remaining in the 160-mL space of the glass vacuum line include H_2, He, Ne and a non-zero but minor vapor pressure of N_2 – all these gases are mass-resolvable from each other on the mass spectrometer, so trace abundances are unlikely to lead to systematic errors in hydrogen isotope measurements.

We tested four different approaches to condensing and trapping these remaining gases into a volume as small as possible (to avoid losing sample during gas expansion into the 50-mL mass spectrometer bellow) and repeated each process multiple times to document whether sample handling on the vacuum

line fractionates the gas in δD and/or ΔDD compositions. These experiments were all made with the same bottle of pure gas used for the quantification of long-term uncertainty (section 5).

In the first series of tests, an aliquot of pure H_2 was expanded into the vacuum line, exposed to the 20-K cold trap, and cryogenically transferred from a large fraction of the vacuum line (160 mL) to a small sample finger (around 2 mL, equipped with a polytetrafluoroethylene (PTFE)-barrelled, threaded stopcock valve) using 5 Å molecular sieve immersed in liquid nitrogen (LN_2 at 77 K) and a transfer time of around 5 min. The molecular sieve was initially preheated under vacuum using a natural-gas torch until baseline pressures were reached (typically <10 mPa). This process resulted in an acceptable yield of H_2 recovered (up to 99 %), measured barometrically. We initially attempted to evacuate this sample finger with the Hg diffusion pump and rotary pump vacuum system before isolating it from the line (i.e., while H_2 was still cryogenically trapped on 77 K molecular seive). This resulted in very large (hundreds of ‰) D-enrichment of the remaining fraction, but with no substantial change in ΔDD (n =6, purple dots on Fig. 6). The δD and ΔDD values of the remaining fraction diverge significantly from what would be expected if the loss of sample H_2 was rate-limited by gas-phase diffusion and underwent Rayleigh distillation. We speculate that this fractionation is instead controlled by a vapor-pressure isotope effect for H_2 sorbed on the molecular sieve at liquid-nitrogen temperature during pumping, though this would require that the vapor pressure effect for DD/HH is fortuitously very nearly twice that for the HD/HH ratio; this too is an attractive target for future laboratory experimental study.

In the second series of test, we reproduced the same protocol from the first tests, but without evacuating the sample finger before isolating the sample finger tube from the rest of the vacuum line. This procedure resulted in a good H_2 recovery (up to 99 %) and subtle shifts in δD spanning a range of 6±3 ‰ (1 σ), inconsistently shifting to both higher and lower values (n=4 – red squares on Fig. 6). Importantly, for our purposes, no significant shift was observed in ΔDD values.

The third series of tests consisted of compressing the H_2 sample into a smaller volume (around 10 mL), using a Toepler mercury pump, followed by trapping it in a sample finger tube (2 mL) using molecular sieve at liquid nitrogen temperature. This process also resulted in smaller shifts of δD (total range 3 ±1.5 ‰) with no significant shift in ΔDD values (n=3; yellow squares on Fig. 6). Finally, we tried to compress the H_2 sample into a 10-mL bulb using the Toepler pump only, i.e., without trapping it on molecular sieve immersed in liquid nitrogen. This protocol did not generate any significant changes in δD or ΔDD values (n=2; green circles in Fig. 6) but led to a loss of around 50 % of our sample relative to the other methods, given the dead space on the vacuum line, combined with 40 % sample waste during gas expansion from the 33-mL bulb into the 50-mL bellow of the mass spectrometer.

We conclude that the collection of H_2 using a molecular sieve cooled at 77 K directly from a large volume of the line (without compressing with Toepler pump or evacuating by vacuum pumps) is the best compromise to recover a significant fraction of H_2, with a yield up to 99 %, undisturbed ΔDD signature (within error), and only minor (<5 ‰) changes to the δD. We adopt this method to extract and collect H_2 from our experimental and natural samples in this study. However, studies focused on exceptionally high accuracy of δD measurements on samples of natural H_2 should consider the methods using a Toepler pump to pre-concentrate gas into a more restricted volume.

8. Clumped isotope systematics of H_2 from abiotic and biological laboratory experiments

8.1. Non-linear mixing effects

Mixing can cause a non-linear effects on the clumped isotope signature (i.e., where the Δ value of the mixture does not reflect the weighted sum of the values of the end members) because clumped isotope compositions are reported relative to a stochastic reference frame, which does not vary linearly with bulk isotopic content (Eiler and Schauble, 2004; Eiler, 2007; Yeung *et al.*, 2012). The isotope effects of mixing can be calculated accurately, assuming the end members are known. Therefore, mixing experiments provide an opportunity to examine our capability to measure known isotopic variations

with relatively little uncertainty in expected outcomes, potentially across a wide range of isotopic compositions. In this section, we report results of isotopic measurements of three mixing experiments where each use two isotopically different H_2 gases as endmembers, and compare the results to theoretical model of non-linear mixing effects in the ΔDD_{ARF} vs. δD composition space (Fig. 7). Each of the three mixing experiments share a common endmember gas, corresponding to our intra-laboratory reference gas, implying that all the mixture curves should converge at one end toward the same point in the plotted composition space. A numerical model was built to simulate and quantify the effects of mixing on combined δD and ΔDD composition (the model is provided in the supplementary data) and compare it to our experiment data. The magnitude of the nonlinear mixing effect on ΔDD is dependent on the bulk isotope composition (δD) and ΔDD values of the endmembers. Specifically, the larger the disparity in δD between the endmembers, the more pronounced the offset in ΔDD compared to a line joining the endmembers in the plotted composition space. Note that during mixing, absolute abundances of HD, HH and DD isotopologues are conserved and the departure of ΔDD from the straight-line relationship reflects the fact that ΔDD is reported relative to the DD/HH ratio for the stochastic distribution at the sample's δD value, and that ratio varies non-linearly with δD. The three pairs of mixing endmembers were chosen to create a large variation in potential ΔDD excesses (i.e., relative to the straight-line mixing relationship), due to a range in contrasts in δD between endmembers: $\Delta\delta$D =8 ‰ for the experiment plotted with green dots, $\Delta\delta$D =237 ‰ for that plotted with blue dots, and $\Delta\delta$D =611 ‰ for that plotted with red dots.

Fig. 7 shows the isotopic compositions measured for each family of mixtures at different mixing ratios, and their associated ΔDD enrichments compared to linear trends between their end members. The measured ΔDD compositions for all mixtures fall within one standard error of the predicted mean model result (Fig. 7). These experiments and their consistency with model predictions show: First, the absolute ΔDD value of our working gas (+233.5 ‰), previously defined using only heating gas experiments, is accurate. Any over- or under-estimation of its clumped isotope composition (by 10 ‰ or more) would have modified the curvature of the three ΔDD vs. δD mixing models and generated a mismatch between measured and modeled data. Second, a gas sample with δD composition as low as –750 ‰ (and natural abundance of DD of around 1 ppb) can be accurately measured in a ΔDD vs. δD composition space. Third, this demonstration shows that not only mixing does not follow linear trends in the plotted composition space, but that it can significantly affect equilibrium temperature reconstructions and potentially lead to temperature overestimates, particularly when H_2 end members of highly contrasting isotopic composition are mixed.

8.2. Isotopic exchange between water and H_2 vapor without catalysts

Uncatalyzed isotope exchange between H_2 and H_2O can be relatively fast at laboratory and geological timescales, at least under some circumstances. When dissolved H_2 is undersaturated in water (i.e., with respect to free, pure H_2 vapor), and no gas phase exists in the headspace of a water-filled vessel, the δD of H_2 has been shown to reach equilibrium with that of H_2O in less than 500 days at 22 °C and around 14 days at 97 °C (Pester *et al.* 2018). However, relatively little is known about the rate of hydrogen isotope exchange between an headspace of H_2 and water, where the low solubility of H_2 may be a significantly limiting factor, and even less is known about the capacity of liquid water to permit co-existing H_2 to approach internal isotopic equilibrium with respect to eq. 1. These questions are relevant for this study, because we wished to explore the isotope systematics, including clumped isotope effects, in H_2 gas subjected to uptake by microbial organisms held in a liquid water medium (section 8.3) and natural H_2 samples collected from water-rich environments (section 9). Therefore, we conducted a simple experiment examining the rates of isotopic exchange between free H_2 vapor and water. Specifically, an aliquot of H_2 gas was held at a pressure of 1bar in a 1-L bulb initially filled with around 100 mL of tap water (δD_{VSMOW} around –65 ‰). We then heated this system at a constant temperature of 80 °C and monitored the ΔDD and δD composition of the gas fraction through time. We chose an initial H_2 with enriched δD and ΔDD compositions to increase the relative amplitude of isotopic shifts associated with exchange. After more than 500 h of monitoring, no significant change of ΔDD or δD was observed (Fig. S3). We infer that gaseous H_2 is essentially non-exchangeable with liquid water (or itself, through eq. 1) under these conditions, perhaps due to its low solubility in water. It follows that

isotopic exchange with water or clumped isotope shifts in H_2 vapor exposed to liquid water do not occur under the conditions and timescales of microbial culturing experiments presented in section 8.3, below.

8.3. Molecular hydrogen consumption – and trace gross production - by methanogens

Molecular hydrogen is a highly potent reductant that can be used as an energy source for diverse microbial forms of life in various ecosystems on Earth, such as hydrothermal vent fields or the deep biosphere, and perhaps beyond the Earth (Petersen et al., 2011; Hellevang et al., 2011; Brazelton et al., 2012; Glein and Zolotov, 2020; Ménez, 2020). In addition, H_2 is a target for energy storage in saline cavities and other depleted oil and gas reservoirs *(e.g.,* Lord et al., 2014) in which activity of hydrogenotrophic metabolisms, including sulfate reduction or methanogenesis, might consume it for energy and convert H_2 into H_2S and CH_4 in the subsurface. Deciphering the microbial imprint of H_2 consumption and/or production on the clumped isotope composition of residual H_2 could provide important new tools for study of these systems. Specifically, we would like to understand whether clumped isotope measurements of molecular hydrogen can be used to recognize biogenic H_2 consumption and/or production, quantitatively constrain the strengths of source and sinks of H_2, and perhaps characterize the specific environments in which H_2 is biologically formed or consumed. We focused our work on H_2/CO_2 dependent methanogenesis, a metabolic strategy which follows a multiple-step pathway that can be abstracted to the following net reaction (noting that the stoichiometric balance of H atoms should not be interpreted as meaning that H from H_2 is directly transferred to CH_4):

$$CO_2 + 4H_2 \rightarrow CH_4 + 2H_2O \quad \text{(eq. 10)}$$

H_2 consumption by methanogens, as well as many other microorganisms, is performed by hydrogenase enzymes which employ a heterolytic cleavage mechanism to reversibly interconvert molecular hydrogen to protons and electrons (e.g., Schulter et al., 2016). The reduction of CO_2 into methane is performed with electrons provided from H_2 oxidation but those electrons are transported through a relatively complex electron transfer chain that involves multiple steps and types of hydrogenases (Fig. 8). However, because the oxidation of H_2 by those hydrogenases is highly reversible, it promotes hydrogen isotopic exchange between H_2 and H_2O (Farkas et al., 1934; Arp and Burris, 1982; Valentine et al., 2004; Löffler et al., 2019), with a net effect that can be described as:

$$H_2 + DOH \leftrightarrow HD + HDO \leftrightarrow D_2 + H_2O \quad \text{(eq. 11)}$$

As a result, the net hydrogen isotopic fractionation associated with hydrogenotrophy is assumed to include both kinetic (eq. 10) and equilibrium (eq. 11) isotope effects, with the later dominating the gross H_2 flux, despite optimal laboratory growth conditions with relatively high H_2 partial pressure (e.g., Valentine et al., 2004). Moreover, the extent of reversibility is thought to be controlled by the availability of free energy, with higher reversibility expected under H_2-limiting, low-driving-force conditions (Valentine et al., 2004). By simultaneously observing HD/HH and DD/HH ratios in residual H_2, it may be possible to quantify the relative contributions of these competing isotope effects during progressive H_2 consumption, i.e., by adding a new independent variable that may have different sensitivity to both kinetic (associated with the reaction in eq. 10) and equilibrium isotope effects (associated with the equilibria in eq. 11). It is possible that such measurements could reveal further mechanistic details of these reactions that are obscured by net reaction stoichiometries such as eqs. 10 and 11.

To this end, batch cultures of *Methanococcus maripaludis* were grown in aqueous media at 37 °C under constant agitation (see supplementary data for details) with a headspace filled with a mixture of gaseous H_2 and CO_2 (80:20 v/v). Three aqueous media were prepared for different experimental conditions with δD values of H_2O: −95.6 ‰ for exp. A (δD of water was measured), between +2169 and 2184 ‰ for exp. B, (δD of water was gravimetrically estimated from proportions of normal and labeled water end members) and between +6087 and 6358 ‰ for exp. C (again, gravimetrically determined). The initial stable isotope composition of H_2 supplied in the headspace of exp. A and C was δD = −292 ‰ and

ΔDD_{ARF} = +226±3 ‰, at a total gas pressure of 276 kPa, and for experiment B the headspace gas had δD = −121 ‰, ΔDD_{ARF} +1000±22 ‰, at a total gas pressure of 192 kPa. These varying initial conditions were chosen to generate distinct trajectories of ΔDD_{ARF} and δD composition during methanogenic net H_2 consumption, which should help us distinguish the different processes of uptake, equilibration, and mixing. During reaction progress, each batch of aqueous media was constantly agitated and monitored by measuring optical density at 600 nm wavelength (OD_{600}). After some period observing culture growth, reaction progress was inhibited by injecting 1M aqueous NaOH. Once the reaction stopped, the remaining H_2 in the headspace was extracted, purified, and measured by IRMS within several of hours to minimize H_2 leaking from the vial and associated opportunities for isotopic fractionation. The molecular composition of residual gas extracted from the headspace was also analyzed by gas chromatography coupled with thermal conductivity detector (GC-TCD). Data from each of the three set of experiments are shown in Fig. 9.

In each set of experiments, we observed consistent trends of cell density increasing and methane production through the course of the experiment. The δD value of H_2 changed relative to the source gas and approached isotopic equilibrium with H_2O regardless of whether the initial δD value of H_2 was higher or lower than the equilibrium value (no change in δD or ΔDD_{ARF} was observed during uninoculated control experiments; see Fig S3 and section 8.2). The δD evolution of H_2 depends primarily on the δD of the H_2O media, an observation consistent with previous studies (e.g., Valentine et al., 2004; Löffler et al., 2019), which hypothesized that hydrogen exchange between water and H_2 is catalyzed by hydrogenase enzymes and is the dominant process modifying the δD value of H_2. On the other hand, ΔDD_{ARF} exhibits a variety of evolutionary trends across the three sets of experiments, in a fashion that might appear counter-intuitive at first glance: In experiment A, ΔDD started at a near-equilibrium value (i.e., close to equilibrium at the temperature of the experiment) and increased monotonically throughout the course of the experiment. In experiment B, ΔDD started at around 1000‰ and decreased monotonically to reach equilibrium near the end of the experiment. In experiment C, ΔDD started near equilibrium, rose during the early part of the experiment, and then fell to lower values, re-approaching equilibrium, towards the end of the experiment.

This third experiment (panel 9C) provides the clearest expression of what we consider to be the most significant new information provided by ΔDD measurements of H_2 residual to microbial methanogenesis: This variable is driven toward equilibrium at the conditions of the experiment, but does so through a path that is not directly proportional to the equilibration of δD, depends strongly on the contrast in δD between starting and ending compositions of residual H_2, and in some cases can even result in changes in direction of evolving ΔDD between the beginning and end of H_2 consumption. We show below that this counter-intuitive behavior provides independent and relatively direct confirmation of a core concept in previous models of the mechanisms of hydrogenotrophic methanogenesis.

We attempt to describe the experimental results in Fig. 9 using an iterative numerical model that simulates the gross uptake (i.e., forward reaction of hydrogenotrophy) and release (i.e., backward reaction) of H_2 (see supplementary data for details). We formulate this model using concepts and specific variables from a previous model designed to explain the evolution in δD of H_2 during hydrogenotrophic methanotropy (Valentine et al., 2004). In this model, H_2 reacts with hydrogenases with two associated kinetic isotope effects that describe the differences in the rate of this reaction between HD and HH ($^{HD}KIE_c$, see Appendix B. for definitions) and between DD and HH ($^{DD}KIE_c$, which we parameterize through the relationship: $^{DD}KIE = \gamma \bullet {}^{HD}KIE^2$, such that the variable γ indicates the direction and strength of the departure of ^{DD}KIE from the value it would have if each D substitution contributed equally to an isotopologue's KIE). Simultaneous to this gross reaction of H_2, there is a counter-flux of new H_2 production that presumably occurs by enzymatic back-reaction of protons sourced from water. Following Valentine et al. (2004), the relative rate of this counter flux is described using the 'efficiency' (E) of hydrogenases, such that E tends to a value of 1 when the reducing potential of H_2 gross uptake by hydrogenases is quantitatively used to reduce CO_2 into CH_4.

Model results successfully reproduced isotopic and compositional trends (Fig. 9). The optimized efficiency E values are about 0.6 for experiments A and C, and 0.35 for experiment D, and are at the

higher end of Valentine et al. (2004)'s estimated range (0.1–0.55). In contrast, our average $^{HD}KIE_c$ value of 1.07 is lower than that estimated by Valentine et al. (1.16-1.45). Overall, relatively high efficiency and low $^{HD}KIE_c$ values are consistent with fast metabolic rates during optimal exponential growth under non-limiting H_2 concentration because of the high H_2 partial pressure used in our experiments. Additionally, the difference in culturing techniques (*i.e.*, open vs. closed systems), studied methanogenic strains and growth phase can affect the comparison of E and $^{HD}KIE_c$ values (Valentine et al., 2004). Among those, the evolution of growth phase during our batch cultures might explain the mismatch between experimental data and model, especially for the few datapoints that were collected toward the end of exponential growth phase in experiments A and C, which are the less well fit by our model (Fig. 9).

The upward trends of ΔDD_{ARF} in experiment A and C are mainly attributed to mixing isotope effects with progressive addition of H_2 molecules with clumped isotope compositions corresponding to apparent equilibrium at the cell growth temperature (37 °C; ΔDD_{ARF} = 217 ‰). In these two sets of experiments, the backward reaction releases H_2 strongly different in δD from the residual H_2 (this is also evidenced by the shift in δD over the experiments), therefore incurring significant non-linearity clumped isotope effects of mixing (Eiler and Schauble 2004). Experiment B is best fitted with a lower value of efficiency, E, which, again, could be related to this experiment's lower H_2 partial pressure. In Experiment B, the δD values of back-released H_2 are more closely similar to those of residual H_2, so ΔDD_{ARF} follows a downward trajectory towards equilibrium.

Our results independently confirm the prior hypothesis that consumption of H_2 by hydrogenases used by hydrogenotrophic methanogens is accompanied by partial back-reaction that generates H_2 from water-sourced protons, partially offsetting the gross influx of H_2 consumption. The H_2 formed by this back reaction is created in equilibrium with water with respect to δD, and internally with respect to ΔDD at the local temperature of the reaction. The uptake reaction, in contrast, can be considered irreversible and associated with kinetic isotope effects that discriminate against HD and D_2. We note that H_2 partial pressure in the natural environment (e.g., Lin et al., 2012) is expected to be significantly lower than in our laboratory experiments (>100 kPa), which should result in a lower free energy of reaction in the natural setting, thus favoring enzymatic reversibility and making the back-flux of produced, equilibrated H_2 proportionally more significant (Valentine et al., 2004). As a result, we should expect environmental H_2 in settings of active hydrogenotrophic methanogenesis may closely approach or reach equilibrium of both δD (with respect to environmental water) and clumped isotopes. Our results further prove that microbial activity is a potent catalyst for hydrogen isotope equilibrium between H_2 and water at moderate to low temperature (<110 °C). Notably, the distinctive non-linear evolution arrays in the δD vs. ΔDD_{ARF} composition space may help in quantifying the extent of microbial H_2 (re)cycling in the environment. Better constraints on subsurface microbial consumption of H_2 should also help us gauge microbial production of CH_4 and better study the processes impacting long-term geological storage of H_2 (Lord et al., 2014).

9. Natural samples

A critical question for clumped isotope measurements of H_2 in natural samples is whether or not ΔDD_{ARF} values reflect formational temperatures by equilibrium processes, or if they are controlled by kinetics, or some combination of the two, and whether the answers to these questions vary across natural settings and processes. Additionally, once a H_2 gas forms (in isotopic equilibrium or not), it is not known if the sample will preserve the ΔDD_{ARF} value it had when formed or may instead undergo isotopic re-equilibration with itself or other H-bearing compounds, such as water. It has been suggested that isotope equilibrium is attained between H_2 and water at its source, and may undergo re-equilibration as temperature cools during ascent of fluids if the fluid upwelling rate is slow (Pester et al., 2018; Ricci et al., 2022). Therefore, clumped isotope composition of H_2 provides another means to use isotope exchange kinetics and equilibrium to constrain the source and flow dynamics of hydrothermal gases. We present here preliminary data for 7 natural H_2 samples, including 2 samples from high temperature oceanic hydrothermal vents (*Rainbow, Ashadze),* 5 samples from low temperature submarine vents (*Lost-City, including Beehive, Marker 2, Marker 6,* and *Marker 3).* In

hydrothermal circulation associated to mid-oceanic ridges, H_2 is typically thought to derive from serpentinization reactions occurring when seawater interact with ultramafic rocks in the subsurface (e.g. Charlou et al., 2002, 2010; Proskurowski et al., 2006). We also measure a sample from an onshore H_2 -rich reservoir (H_2 fraction up to 90%) from a Neoproterozoic sedimentary basin in Mali (Bourakébougou). The origin of H_2 is less clear and may involve water-rock reactions between meteoric water and basement rocks at depth (Prinzhofer et al., 2018).

As shown on Fig. 10, measured ΔDD_{ARF} values of these natural H_2 samples vary from 225 to 72 ‰, corresponding to a range in apparent temperatures from 27 to 375 °C, respectively. With one exception, all samples overlap within uncertainties the sampling temperature of each site (the exception, *Lost-city-Marker 2*, has an apparent ΔDD_{ARF} equilibrium temperature around 30 °C lower than the temperature of the expelled fluid). We compared these intra-molecular ΔDD_{ARF}-based apparent temperatures with apparent equilibrium temperatures between H_2(g) and H_2O(l) using the δD measured for each sample and estimated for its associated environmental water, and a temperature-dependent isotopic fractionation factor calculated from Horita and Wesolowski's (1994) and Suess (1949). As shown on Fig. 10B, samples from *Mali, Rainbow and Ashadze* fall on the H_2/H_2O equilibrium line at their corresponding ΔDD_{ARF}-based temperature (for a water with $\delta D = 0 \pm 20$ ‰), which is also consistent with their site temperature of 30–40 °C and 350–360 °C, respectively. This is direct evidence that hydrogen exchange between H_2 and H_2O at these localities was also accompanied by equilibration amongst H_2 isotopologues. Hence, both the bulk H isotope and clumped isotope composition reached a self-consistent equilibrium with water at the sampling site.

Interestingly, most samples from *Lost City* display ΔDD_{ARF}-based temperatures between 27 °C and 81 °C, closely similar to venting temperature, but inconsistent with the apparent H_2/H_2O hydrogen isotope equilibrium temperatures (which are systematically higher, between 77 °C and 120 °C; Proskurowski *et al.*, 2006). These findings suggest that cooling fluids may re-equilibrate the internal distribution of H_2 isotopologues to environmental temperature more rapidly than they do the isotopic exchange between H_2O and H_2. The mechanism of this faster re-equilibration among the H_2 isotopologues is unclear. In the laboratory, gaseous H_2 reordered only in the presence of a metal catalyst and our observations of uncatalyzed H_2O-H_2 isotope exchanges indicate that ΔDD_{ARF} value of H_2 in contact with water at 80 °C remained unchanged over a period of 3 weeks. Note that a residence time of 11 days was estimated by Pester *et al.* 2018 in the upflow zone at *Lost City*, where fluid cooled through the temperature range relevant to our observations. Biologically-mediated catalysis by methanogens or sulfate reducers (both of which use H_2 as an electron donor) may drive the H_2 toward near-equilibrium condition with environmental temperatures, as observed in section 8c, but this implies a near-total consumption of the H_2 (i.e., so that H_2 gross production by metabolic 'back reaction' dominates the composition of the residual H_2), which is not in line with the high H_2 concentrations (0.90-14 mmoles H_2/kg) observed at Lost City. Hence, our results imply a metal or other solid or dissolved catalyst that may occur in underlying serpentinites and drive the isotopologues of molecular hydrogen to mutual equilibrium during fluid ascent at Lost City. Focused experimental studies are required to examine this hypothesis further. Our results reveal a relatively faster exchange kinetics for self-exchange of H_2 than between H_2 and H_2O. ΔDD of H_2 could obtain equilibrium at relatively cool temperature (<100 °C) within short time periods (<11 d), while isotope fractionation of H_2O/H_2 remain blocked at >100 ˚C, which is consistent with Ricci et al. (2022). Such differential kinetics extend our capability to track the thermal evolution of these fluids. For example, if future studies show disequilibrium of ΔDD at environmental temperatures, it will indicate an exceptionally fast rate of fluid upwelling and cooling.

Note that a recent study of the proportions of isotopologues of methane effusing at Lost City (Labidi *et al.* 2020) revealed that $^{13}CH_3D$ proportions are consistent with abiotic methane being synthesized at 250–150 °C, whereas $^{12}CH_2D_2$ isotopologue proportions closely match fluid venting temperatures (65–100 °C), and presumably record near complete re-equilibration at post formation fluid venting temperatures, as observed for D_2. This could be a simple coincidence but provides suggestive evidence for preferential re-ordering of doubly deuterated isotopologues ($^{12}CH_2D_2$ and D_2) in both CH_4 and H_2 molecules at rates substantially in excess of their singly deuterated relatives – a peculiar proposition that implies enhanced rates of isotope exchange of the doubly deuterated species, far in excess of what

would be expected from isotopologue symmetry numbers alone (which are limited to factor ~2 differences, see e.g., Giunta *et al.*, 2021). This interpretation would imply a quantum-mechanical rate enhancement of the doubly deuterated species relative to the singly deuterated species — a speculation that calls for further investigation.

10. Conclusions

We report here an improved method to measure the clumped isotope composition of molecular hydrogen through a high-resolution mass spectrometer, in a fashion based on Popa et al. (2018) but modified and tested to document and correct for various analytical and methodological artifacts. We have documented the accuracy of this method through comparison to established methods for the determination of δD values and through measurements of gases that have been driven to intramolecular isotopic equilibrium by heating in the presence of a catalyst. This procedure allowed us to establish a correction scheme to convert ΔDD_{wg} data to a common absolute reference frame based on the theoretical temperature dependence of equilibrium clumping in molecule hydrogen, following the same procedure previously used for clumped isotope study of CO_2 and several other compounds. We then tested our reference frame by comparing theoretical predictions of non-linear mixing effects with measurements of mixtures of isotopic end member gases with varying δD_{VSMOW} and ΔDD_{ARF} values. We also found that vacuum line manipulation of H_2 does not significantly affect the gas ΔDD_{ARF} composition (although care and specific procedures are required to minimize changes in δD_{VSMOW}) opening the way to the first series of measurement of H_2 clumped isotope on natural geological samples. Experiments examining H_2 consumption by methanogens document that the hydrogenotrophy pathway involves both kinetic (eq. 10) and equilibrium (eq. 11) isotope effects. However, the back-release of molecular hydrogen eventually dominates the isotopic composition of the residual H_2 by progressively equilibrating isotopologues both intramolecularly and with water, a process that drives the H_2 ΔDD value toward near equilibrium at environmental temperatures. These findings can be used as a basis to recognize biogenic H_2 consumption and/or production, quantitatively constrain the strengths of sources and sinks of H_2, and perhaps characterize the specific environments in which H_2 is biologically formed or consumed. Our results on natural H_2 samples suggest that clumped isotope ordering in H_2 is highly sensitive to re-equilibration, but records processes not observed in the hydrogen isotope exchange between H_2 and H_2O. Specifically, in environments of significant interest, H_2-H_2O equilibration occurs at systematically higher temperatures than internal clumped isotope equilibration of H_2. More detailed studies of these and other issues, particularly examining the rates of isotope exchange both intramolecularly and between H_2 and H_2O, are required to develop more confident interpretations of the clumped isotope systematic in natural or experimental hydrogen samples.

AKNOWLEGMENT.

We thank Nami Kitchen and Jonathan Treffkorn for assistance with laboratory work associated with the measurements presented here. We are grateful to Alain Prinzhofer and Aliou Boubacar Diallo for giving us access to the natural samples from Mali. Samples from Rainbow and Ashadze hydrothermal fields were collected during Ifremer cruises Exomar (2005) and Serpentine (2007) on board R/V Atalante and R/V Pourquoi Pas?. We thank Jean-Pierre Donval for collecting these samples as well as Anne Godfroy and Yves Fouquet who was leading these campaigns. This study is supported with funds provided by TotalEnergies, Pau, France.

FIGURES CAPTIONS.

Figure 1. DD natural abundance for range of δD (vs. VSMOW) and ΔDD compositions comparable to those expected in geological H_2 samples (c.f., the black bars in top, modified after Hao et al. 2020).

Figure 2. Mass scans on m/z 2 (HH), 3 ($HD+H_3^+$) and 4 ($DD+H_2D^+$) regions for two isotopically different gasses with δD and ΔDD compositions of –124.3/233.5 ‰ for gas 1 and –361.7/108.6 ‰ for

gas 2. Note that all the peak shape scans were performed at the same working pressure, equivalent to 2 x 10^9 counts per second on HH.

Figure 3. Comparison of δD measurements made on the Ultra (horizontal axis) and through conventional techniques (vertical scale). The left panel include samples made through reduction of H_2O to H_2 at Indiana University, while the right panel include isotopically labelled H_2 bottles made and calibrated against international standard between 1992 and 2004. See text for details. The error associated with δD-H2 measurements is less than the width of the plotting symbol in both dimensions.

Figure 4. Summary of data for equilibrated gases generated at Caltech between February and September 2021 on a total of 32 heated gases made from 6 'Oztech' bottles, re-equilibrated at 11 different temperatures. Panel A show linear trends in a plot ΔDD vs. δD measured vs. a common reference gas of constant isotopic composition, measured for gases equilibrated to a single temperature and measured at nearly constant instrument tuning conditions over a period of days. The slopes of these lines (n=7) document the range in non-linearity of response of our mass spectrometer. The X axis on panel B represents the intercept of each heated gas line (ΔDD_0) in panel A while the Y axis represents the theoretical ΔDD values expected at the temperatures of equilibration. The departure of the trend in this Figure from a slope of 1 mostly reflects the compression of the scale of delta values when the DD/HH ratio of the reference gas is used as a normalizing constant (see below). Panel C replots the data from panel B, after using the standard conversion identity to translate the ΔDD_0 values into a reference frame equivalent to that for the working gas's stochastic distribution. Panel D illustrates the translation of our heated gas data into our absolute reference frame (ΔDD_{AE}), plotted versus the oven temperature at which the gasses were equilibrated. For reference the theoretical thermodynamic equilibrium is also illustrated with a red line. The corresponding data used to generate these plots is found in **Table S1** (heated gas section).

Figure 5. 'Long term' monitoring of the δD/ΔDD composition of a sample over a six-month period. Note that the ΔDD were corrected for non-linearity effect and translated into the 'absolute reference frame'.

Figure 6. Monitoring of stable isotope composition (δD and ΔDD) of a bottle of pure H_2, before (black) and after vacuum line manipulation using different handling protocols: purple dots = Molecular sieve at 77 K and pumping, visible in the top panel only; red square = Molecular Sieve at 77 K without pumping; yellow square = Toepler pump and Molecular Sieve at 77 K (no pumping); green dots = only Toepler pump. See text for more detail.

Figure 7. Summary of experimental data and model predictions for three mixing experiments sharing a common endmember corresponding to our reference gas (δD of –124.4 ‰ and ΔDD of +233.5 ‰; black dots). Green, blue and reds squares mark the isotope compositions of the other three endmembers used in the mixtures. Green, blue and reds dots are the mixtures themselves. All ΔDD compositions are translated into the absolute reference frame presented above. Modeled ΔDD and δD values of mixtures are illustrated with open circles, and linear trends between end members with dashed lines.

Figure 8. Simplified hydrogenotrophic methanogenesis pathway and interactions between hydrogen and hydrogenases. a. Overall pathway where H_2 is dissolved from the headspace into the media. The hydrogenases catalyze a reversible conversion of molecular hydrogen to protons and electrons either at the periplasm or in the cytoplasm. The reducing potential of this reaction can be transferred further down through electron chain transport with electron acceptors such as ferredoxin or F420 to reduce CO_2 into methane through a multistep process (Thauer et al., 2010). b. Representation of a hydrogenase during net uptake of H_2. c. Representation of back flux (fh in the model) of H_2. The net reaction of panels b and c represents the gross uptake flux of H_2 binding to hydrogenases (fc).

Figure 9. Left panels. Temporal evolution of ΔDD_{ARF}, δD in the head space and cell density (OD_{600}) in the media during growth of *M. maripaludis* in batch culture experiments with different initial conditions (A, B and C; see text for details). Each of these experiments has an expected δD of H_2 in equilibrium with water of ~ –772 ‰, –195±10 ‰ and +860±40 ‰, respectively. Right panels: Relationship between of ΔDD_{ARF} and δD_{VSMOW} and the remaining fraction of H_2 (calculated as $f\text{-}H_2 = V_{H2} / (V_{H2} + 4V_{CH4})$, note that this equation neglects H_2 consumption for anabolism). Model results are shown as red (exp A), black (exp B) and blue (exp C) lines and represent the best match to three adjustable parameters, efficiency (E), forward reaction KIE for HD (^{HD}KIE) and forward reaction clumped isotope KIE (γ). These parameters are identical for the three set of experiments, except for efficiency parameter of scheme B, which we allow to be different from E of experiments A and C, because experiment B has a different H_2 headspace pressure. See text and Appendix 2 for detail and model sensitivity test.

Figure 10. Summary of the δD_{VSMOW} and ΔDD_{ARF} values of H_2 from various natural samples. **A**. Sample geographical locations. **B**. Clumped isotope composition of H_2 plotted versus the venting (for submarine hydrothermal vents) or reservoir (Mali) temperatures at the sampling sites. Blue dots are samples from Lost City, black and grey dots are from Rainbow and Ashadze, respectively, and the red dot is a datum from a Malian reservoir (Bourakébougou). **C**. ΔDD_{ARF} versus δD_{VSMOW} values of natural samples, plotted together with the $H_2(g)/H_2O(l)$ equilibrium field calculated for waters with a δD_{VSMOW} of 0 ±20 ‰.

REFERENCES

Arp D. J. and Burris R. H. (1982) Isotope exchange and discrimination by the H_2-oxidizing hydrogenase from soybean root nodules. *Biochim. Biophys. Acta BBA - Protein Struct. Mol. Enzymol.* **700**, 7–15.

Brazelton W., Nelson B. and Schrenk M. (2012) Metagenomic evidence for H_2 oxidation and H_2 production by serpentinite-hosted subsurface microbial communities. *Front. Microbiol.* **2**, 268.

Charlou J. L., Donval J. P., Fouquet Y., Jean-Baptiste P. and Holm N. (2002) Geochemistry of high H_2 and CH_4 vent fluids issuing from ultramafic rocks at the Rainbow hydrothermal field. *Chem. Geol*. **191**, 345–359.

Clog M., Lawson M., Peterson B., Ferreira A. A., Santos Neto E. V. and Eiler J. M. (2018) A reconnaissance study of ^{13}C–^{13}C clumping in ethane from natural gas. *Geochim. Cosmochim. Acta* **223**, 229–244.

Craig H. (1957) Isotopic standards for carbon and oxygen and correction factors for mass-spectrometric analysis of carbon dioxide. *Geochim. Cosmochim. Acta*, **12**, 133-149.

Dennis K. J., Affek H. P., Passey B. H., Schrag D. P. and Eiler J. M. (2011) Defining an absolute reference frame for 'clumped' isotope studies of CO_2. *Geochim. Cosmochim. Acta* **75**, 7117–7131.

Dong G., Xie H., Kitchen N., Formolo M. J., Michael L., Sessions A. L. and Eiler J. M. (2021) Clumped isotope effects of thermogenic methane formation: Insights from pyrolysis of hydrocarbons. *Geochim. Cosmochim. Acta* **303**, 159–183

Dong, G., Xie, H., Formolo, M., Lawson, M., Sessions, A. and Eiler, M. (2021). Clumped isotope effects of thermogenic methane formation: Insights from pyrolysis of hydrocarbons. *Geochimica et Cosmochimica Acta*. **303**, 159-183.

Eberle U, Felderhoff M and Schüth F. (2009) Chemical and physical solutions for hydrogen storage. *Angew Chem Int Ed Engl*. **48**, 08-30.

Ehhalt, H. and Rohrer. F. (2009). "The tropospheric cycle of H_2: a critical review." *Tellus B: Chemical and Physical Meteorology.* **61,** 500 - 535.

Eiler J. M. (2007) "Clumped-isotope" geochemistry – the study of naturally-occurring, multiply-substituted isotopologues. *Earth Planet. Sci. Lett.* **262**, 309–327.

Eiler J. M. (2011) Paleoclimate reconstruction using carbonate clumped isotope thermometry. *Quatern. Sci. Rev*. **30**, 3575– 3588.

Eiler J. M. (2013) The isotopic anatomies of molecules and minerals. *Annu. Rev. Earth Planet. Sci*. **41**, 411–441.

Eiler J. M. and Schauble E. (2004) $^{18}O^{13}C^{16}O$ in Earth's atmosphere. *Geochim. Cosmochim. Acta*. **68**, 4767–4777.

Eiler J. M., Clog M., Magyar P., Piasecki A., Sessions A., Stolper D., Deerberg M., Schlueter H.-J. and Schwieters J. (2013) A high-resolution gas-source isotope ratio mass spectrometer. *Int. J. Mass Spectrom*. **335**, 45–56.

Etiope G. and Sherwood Lollar B. (2013) Abiotic methane on Earth. *Rev. Geophys*. **51**, 276–299.

Farkas A., Farkas L., Yudkin J. and Rideal E. K. (1934) The decomposition of sodium formate by bacterium coli in the presence of heavy water. *Proc. R. Soc. Lond. Ser. B Contain. Pap. Biol. Character* **115**, 373–

379.
Gould AJ, Bleakney W, Taylor HS. (1934) The inter-relations of hydrogen and deuterium molecules. *J Chem Phys.* **2**, 362-373.
Glein C. R. and Zolotov M. Yu. (2020) Hydrogen, Hydrocarbons, and Habitability Across the Solar System. *Elements* **16**, 47–52.
Hallenbeck, P.C., Benemann, J.R., (2002). Biological hydrogen production : fundamentals and limiting processes. *International Journal of Hydrogen Energy*. **27**,11–12.
Hao, Y., Pang, Z., Tian, J., Wang, Y., Li, Z. and Li, L., (2020). Origin and evolution of hydrogen-rich gas discharges from a hot spring in the eastern coastal area of China. *Chemical Geology***. 538**, 119-177.
Hellevang H., Huang S. and Thorseth I. H. (2011) The Potential for Low-Temperature Abiotic Hydrogen Generation and a Hydrogen-Driven Deep Biosphere. *Astrobiology* **11**, 711–724.
Horita J. and Wesolowski D. J. (1994) Liquid-vapor fractionation of oxygen and hydrogen isotopes of water from the freezing to the critical temperature. *Geochim. Cosmochim. Acta***. 58**, 3425– 3437.
Huntington K., Eiler J., Affek H., Guo W., Bonifacie M., Yeung L., Thiagarajan N., Passey B., Tripati A. and Daëron M. (2009). Methods and limitations of 'clumped' CO_2 isotope (Δ_{47}) analysis by gas-source isotope ratio mass spectrometry. *J. Mass Spectrom*. **44**, 1318–1329
Labidi, J., Barry, P.H., Bekaert, D.V. *et al.* (2020) Hydrothermal $^{15}N^{15}N$ abundances constrain the origins of mantle nitrogen. *Nature* **580,** 367–371.
Labidi, J., Young, E.D., Giunta, T., Kohl, I.E., Seewald, J., Tang, H., Lilley, M.D., Früh-Green, G.L. (2020). Methane thermometry in deep-sea hydrothermal systems: Evidence for re-ordering of doubly-substituted isotopologues during fluid cooling. *Geochimica et Cosmochimica Acta*. **288**, 248-261.
Lin, L.H., Slater, G.F., Lollar, B.S., Lacrampe-Couloume, G. and Onstott, T.C. (2005). The yield and isotopic composition of radiolytic H_2, a potential energy source for the deep subsurface biosphere. *Geochimica et Cosmochimica Acta*, **69**, 893-903.
Lin, Y. S., Heuer, V. B., Goldhammer, T., Kellermann, M. Y., Zabel, M., & Hinrichs, K. U. (2012). Towards constraining H2 concentration in subseafloor sediment: a proposal for combined analysis by two distinct approaches. *Geochimica et Cosmochimica Acta*, *77*, 186-201.
Löffler, M., Kümmel, S., Vogt, C. and Richnow H.H., (2019). H_2 Kinetic Isotope Fractionation Superimposed by Equilibrium Isotope Fractionation During Hydrogenase Activity of D. vulgaris Strain Miyazaki. *Frontiers in Microbiology.* **10,** 15-45.
Lord A. S., Kobos P. H. and Borns D. J. (2014) Geologic storage of hydrogen: Scaling up to meet city transportation demands. *Int. J. Hydrog. Energy* **39**, 15570–15582.
Loyd, M., Eldrige, D., Solper, D. (2020). Clumped $^{13}CH_2D$ and $^{12}CHD_2$ compositions of methyl groups from wood and synthetic monomers: methods, experimental and theoretical calibrations, and initial results. *Geochimica et Cosmochimica Acta*. **297**, 233-275
Magyar, P. M., Orphan, V. J., and Eiler, J. M. (2016). Measurement of rare isotopologues of nitrous oxide by high-resolution multi-collector mass spectrometry. *Rapid Communications in Mass Spectrometry*. ***30***, 1923-1940.
Mangenot, X., Tarantola, A., Mullis, J., Girard, J. P., Le, V. H., and Eiler, J. M. (2021). Geochemistry of clumped isotopologues of CH_4 within fluid inclusions in Alpine tectonic quartz fissures. *Earth and Planetary Science Letters*. **561**, 116792.
Ménez, B. (2020). Abiotic Hydrogen and Methane: Fuels for Life. *Elements*. **16**, 39-46.
Nandi, R. and Sengupta, S. (1998). Microbial production of hydrogen: an overview. Critical Reviews in *Microbiology*. **24**, 61–84.
Palla, F; Salpeter, E E and Stahler, S W (1983). Primordial star formation - The role of molecular hydrogen. *Astrophysical Journal.* **271**,632-641.
Petersen J. M., Zielinski F. U., Pape T., Seifert R., Moraru C., Amann R., Hourdez S., Girguis P. R., Wankel S. D., Barbe V., Pelletier E., Fink D., Borowski C., Bach W. and Dubilier N. (2011) Hydrogen is an energy source for hydrothermal vent symbioses. *Nature* **476**, 176–180.
Pester, N.J., Conrad, M.E., Knauss, K.G., DePaolo, D.J., (2018) Kinetics of D/H isotope fractionation between molecular hydrogen and water. *Geochimica et Cosmochimica Acta*. **242**, 192-212.
Piasecki, A., Sessions, A., Peterson, B. Eiler, J. (2016). Prediction of equilibrium distributions of isotopologues for methane, ethane and propane using density functional theory. *Geochimica et Cosmochimica Acta*. **190**, 1-12.
Popa, M.E., Paul, D., Janssen, C. and Röckmann, (2019). H_2 clumped isotope measurements at natural isotopic abundances. *Rapid Communications in Mass Spectrometry*. **33**, 239–251.
Prinzhofer, A., Cissé, S.S.T. and Diallo, A.B. (2018). Discovery of a large accumulation of natural hydrogen in Bourakebougou (Mali). *International Journal of Hydrogen Energy*. **43**, 19315–19326.
Proskurowski G., Lilley M. D., Kelley D. S. and Olson E. J. (2006) Low temperature volatile production at the Lost City Hydrothermal Field, evidence from a hydrogen stable isotope geothermometer. *Chem. Geol.*

229, 331–343.
Reeves, E.P. and Fiebig, J., (2020). Abiotic synthesis of methane and organic compounds in Earth's lithosphere. *Elements.* **16**, 25–31.
Ricci A., Kleine B.I., Fiebig J., Gunnarsson-Robin J., Kamunya K.M., Mountain B., Stefánsson A. 2022. Equilibrium and kinetic controls on molecular hydrogen abundance and hydrogen isotope fractionation in hydrothermal fluids. Earth and Planetary Science Letters. 579, 117-138
Rittenberg D, Bleakney W and Urey HC. (1934) The equilibrium between the three hydrogens. *J Chem Phys*. **2**, 48-49.
Röckmann T., Popa M. E., Krol M. C. and Hofmann M. E. G. (2016) Statistical clumped isotope signatures. *Sci Rep*. **6,** 31-47.
Schilter D., Camara J. M., Huynh M. T., Hammes-Schiffer S. and Rauchfuss T. B. (2016) Hydrogenase Enzymes and Their Synthetic Models: The Role of Metal Hydrides. *Chem. Rev*. **116**, 8693–8749.
Sessions A. L., Burgoyne T. W. and Hayes J. M. (2001) Determination of the H^3 factor in hydrogen isotope ratio monitoring mass spectrometry. *Anal. Chem*. **73**, 200–207.
Sherwood Lollar, B.**,** Voglesonger, K.**,** Lin, L.-H.**,** Lacrampe-Couloume, G.**,** Telling, J.**,** Abrajano, T.A.**,** Onstott, T.C. and Pratt**,** L.M. (2007). Hydrogeologic controls on episodic H_2 release from Precambrian fractured rocks—Energy for deep subsurface life on Earth and Mars. *Astrobiology*. **7,** 971-986.
Shull, J.M and Beckwith, S. (1982). Interstellar molecular hydrogen. Ann. Rev. *Astron. Astrophys*, **20**, 163-90.
Stolper, D.A., Sessions, A.L., Ferreira, A.A., Santos Neto, E.V., Schimmelmann, A., Shusta, S.S., Valentine, D.L., Eiler, J.M., (2014). Combined ^{13}C-D and D-D clumping in methane: methods and preliminary results. *Geochim. Cosmochim. Acta***. 126**, 169–191.
Suess H. E. (1949) Das Gleichgewicht H2 + HDO, HD+H2O und die weiteren austauschgleichgewichte im system H2, D2 und H2O. Z. *Naturforsch*. **4**, 328–332.
Thauer RK, Kaster AK, Goenrich M, Schick M, Hiromoto T, Shima S. (2010). Hydrogenases from methanogenic archaea, nickel, a novel cofactor, and H_2 storage. Annu Rev Biochem.79, 507-36.
Tissot, B.P. and Welte, D.H. (1984) Petroleum Formation and Occurrence. Springer-Verlag, Berlin.
Truche, L., McCollom, T.M. and Martinez, I., (2020). Hydrogen and abiotic hydrocarbons: molecules that change the world. *Elements*. **16**, 13–18.
Urey HC (1947). The thermodynamic properties of isotopic substances. *J Chem Soc*. 562-581.
Valentine D. L., Chidthaisong A., Rice A., Reeburgh W. S. and Tyler S. C. (2004) Carbon and hydrogen isotope fractionation by moderately thermophilic methanogens. *Geochim. Cosmochim. Acta***. 68**, 1571–1590.
Walshe, J., Neumayr, P. and Halley, S., (2006). Fluids in the system. In: Walshe, J., Neumayr, P. and Petersen, K. (eds.), Scale-integrated, architectural and geodynamic controls on alteration and geochemistry of gold systems in the Eastern Goldfields Province, Yilgarn Craton. Minerals and Energy Research Institute OF Western Australia, Project M358, Report **256**, 29–72.
Wang Z., Schauble E. A. and Eiler J. M. (2004) Equilibrium thermodynamics of multiply substituted isotopologues of molecular gases. *Geochim. Cosmochim. Acta***. 68**, 4779–4797.
Wang, D., et al. (2015). Nonequilibrium clumped isotope signals in microbial methane. Science **348**, 428-431.
Xie, H., Dong, G., Formolo, M., Lawson, M., Liu, J., Cong, F., Mangenot, X., Shuai, Y., Ponton, C. and Eiler, J. (2021). The evolution of intra-and inter-molecular isotope equilibria in natural gases with thermal maturation. *Geochimica et Cosmochimica Acta*. ***307***, 22-41.
Xie, H., Ponton, C., Formolo, M. J., Lawson, M., Ellis, G. S., Lewan, M. D., Ferreira, A., Morais, E.T., Spigolon, A.L., Sessions, A. and Eiler, J. M. (2020). Position-specific distribution of hydrogen isotopes in natural propane: Effects of thermal cracking, equilibration and biodegradation. *Geochimica et Cosmochimica Acta*. ***290***, 235-256.
Xie, H., Ponton, C., Formolo, M. J., Lawson, M., Peterson, B. K., Lloyd, M. K., Session, A. and Eiler, J. M. (2018). Position-specific hydrogen isotope equilibrium in propane. *Geochimica et Cosmochimica Acta*. ***238,*** 193-207.
Yeung L. Y. (2016) Combinatorial effects on clumped isotopes and their significance in biogeochemistry. *Geochim. Cosmochim. Acta.* **172**, 22–38.
Yeung L. Y., Young E. D. and Schauble E. A. (2012) Measurements of $^{18}O^{18}O$ and $^{17}O^{18}O$ in the atmosphere and the role of isotope-exchange reactions. *J. Geophys. Res*. **117,** 114-129.
Yeung, L., Li, S., Kohl, I., Haslun, J., Ostrom, N., Hu, H., Fischer, T., Schauble, E., and Young, E. (2017) Extreme enrichment in atmospheric $^{15}N^{15}N$. *Science Advances*. **3**, 6741.
Young, E.D., et al. (2017). The relative abundances of resolved $^{12}CH_2D_2$ and $^{13}CH_3D$ and mechanisms controlling isotopic bond ordering in abiotic and biotic methane gases. *Geochim. Cosmochim. Acta*. **203**, 235-264.
Zgonnik, V. (2020). The occurrence and geoscience of natural hydrogen: a comprehensive review. *Earth-Science Reviews***. 203**, 103-140.

APPENDIX A - Culturing experiments – Method

Batch cultures of *Methanococcus maripaludis* strains S2 (Jones et al., 1983), supplied by J. A. Leigh from the University of Washington, were cultured at 37 °C under constant stirring at 200 rpm with 80/20 v/v H_2/CO_2 at 267 kPa in the headspace except for experiments B, where the headspace contains H_2 enriched ΔDD and the pressure was 192 kPa. The medium for all experiments contained 18 g of NaCl, 2.75 g of $MgCl_2 \cdot 7H_2O$, 0.34 g of KCl, 3.45 g of $MgSO_4 \cdot 7H_2O$, 0.25 g of NH_4Cl, 0.14 g of $CaCl_2 \cdot 2H_2O$, 0.14 g of K_2HPO_4, 2 mg of $Fe(NH_4)_2(SO_4)_2 \cdot 7H_2O$, 5 g of $NaHCO_3$, 1 g of CH_3COONa, 2 g of trypticase, 2 g of yeast extract, 0.5 g of cysteine-$HCl \cdot H_2O$, 10 mL of trace elements and 10 mL of vitamin solutions per liter. After filter sterilizing (0.2 μm), the medium was sparged with 80/20 v/v N_2/CO_2 or H_2/CO_2 to flush dissolved oxygen and then reduced by injecting 0.5 g/L of $Na_2S \cdot 9H_2O$. The pH was measured and adjusted to 7 if necessary.

The δD of milli-Q water used for the media was measured on a Picarro L2140-i wavelength-scanned cavity ring-down spectroscopy instrument, each measurement consisting of 9 injections. The δD value was calibrated on the VSMOW scale using four internal water standards ranging from –155.2 to 4.0 ‰ VSMOW. The precision and accuracy were better than 0.3 ‰. For experiments B and C, the D content was adjusted by weighted addition of D_2O water (fractional abundance of 99.9 atom %, Sigma Aldrich) to reach the desired isotopic composition and final δD value in each bottle was determined gravimetrically, including the inoculum with an estimated error below 30 ‰ for experiment B and below 10 ‰ for experiment C.

For inoculation, 5 vol. % of pre-cultured cells in exponential phase was used. Cell growth was monitored by measuring optical density at 600 nm wavelength (OD_{600}). Bottles were sacrificed over the course of the experiments by injecting 20 % (v) of 1M NaOH and stored upside down. Following extraction for isotopic analysis, the molecular composition of H_2 and CH_4 in the headspace was analyzed on a gas chromatograph, HP 5890 series II equipped with molecular sieve column (Agilent Mol-siv 5A 30 m 0.320 mm ID) and a thermal conductivity detector (TCD) with N_2 as a gas carrier (2.2 mL/min). Manual injections of 10 to 100 μL were performed in split mode. Oven temperature was kept at 32 °C and TCD at 125 °C. Quantification was performed based on standard curves made from varied content of H_2 and CH_4 standards.

APPENDIX B. Isotopic model of hydrogenotrophic methanogenesis

We constructed an isotopologue-specific numerical model for tracking the evolution of quantity and isotopologue ratios of molecular hydrogen in the culturing experiments presented in this study. The model follows the concepts developed by Valentine et al., 2004 to simulate the uptake and equilibration with water of molecular hydrogen via hydrogenases activity (Fig. S4). In this model, interactions between hydrogenases and dissolved molecular hydrogen are described abstractly, by way of two separate fluxes. A first, f_c denoting the gross uptake flux of H_2 binding to hydrogenases and, a second, f_h representing the reverse reaction of hydrogenases, which produces H_2 from hydrogenase-bound hydrogen that is undergoes rapid isotope exchange equilibrium with water (Fig. S4). It is assumed that the reverse reaction rate is proportional to rate of the forward uptake reaction with $E \in (0,1)$ denoting the hydrogenases efficiency:

$$f_h = (1-E) * f_c.$$

The binding between H_2 and hydrogenase is assumed to be accompanied by hydrogen isotope KIE. We define isotopologue-specific KIE for HD and DD:

$$^{HD}KIE_c = k_c(HH)/k_c(HD),$$

$$^{DD}KIE_c = k_c(HH)/k_c(HD).$$

We denote that $^{DD}KIE_c = \gamma_c {}^{HD}KIE_c^2$, where γ_c is an additional clumped isotope KIE, following nomenclature in previous publications (Wang et al., 2016; Whitehill et al., 2017). Similarly, there are isotopologue-specific KIEs for the release of H_2 from hydrogenase:

$$^{HD}KIE_h = k_h(HH)/k_h(HD),$$

$$^{DD}KIE_h = k_h(HH)/k_h(HD).$$

$^{DD}KIE_h = \gamma_h {}^{HD}KIE_h^2$ is as previously noted. The exchange equilibration between hydrogenase-bound hydrogen and protons in water is treated as an instantaneous process. We assumed HD/HH and DD/HH of hydrogenase-bound hydrogen to be in equilibrium with water. This equilibrium isotope effect (EIE) is treated to be equal to EIE between molecular hydrogen and water using previous calibrations of Horita and Wesolowski (1994) and Suess (1994). This estimated EIE might be different from the true value in our experiments because of the bonds between hydrogenase active site and hydrogen (e.g., Schilter et al., 2016). However, we note that this approximation is acceptable for our modeling purpose because the reverse reaction KIEs ($^{HD}KIE_h$, $^{DD}KIE_h$) are optimizable parameters (also see paragraph in the end of this section for holistic description) that will offset the discrepancy here, as they are multiplied in the final expression

$$[HD/HH]_e = 2[D/H]_{water} \times {}^{HD}EIE,$$

$$[DD/HH]_e = [D/H]_{water}^2 \times {}^{DD}EIE.$$

Since we are sampling and analyzing H_2 in the headspace gas, the model also considers isotopic fractionation of H_2 between the gaseous and the dissolved phase. We use $^{HD}EIE_{aq/g}$ and $^{DD}EIE_{aq/g}$ to denote EIE for HD/HH and DD/HH, respectively. These values are taken from previous experimental studies (Knox et al. (1992) for HD/HH and Muccitelli and Wen (1978) for DD/HH respectively). Based on the preceding description and assumptions, we can model the evolution of isotopologue concentrations with the following ordinary differential equations:

$$d[HH]/dt = -E \times f_c;$$

$$d[HD]/dt = -f_c * [HD/HH]_e / {}^{HD}KIE_c \times {}^{HD}EIE_{aq/g} + (1-E) f_c \times 2[D/H]_{water} \times {}^{HD}EIE / {}^{HD}KIE_h / {}^{HD}EIE_{aq/g};$$

$$d[DD]/dt = -f_c * [DD/HH]_e / \gamma_c {}^{HD}KIE_c^2 \times {}^{HD}EIE_{aq/g} + (1-E) f_c \times [D/H]_{water}^2 \times {}^{DD}EIE / \gamma_h {}^{HD}KIE_h^2 / {}^{DD}EIE_{aq/g}.$$

These series of equations can be solved numerically, and time-evolving concentrations of [HH], [HD] and [DD] are converted to δD and ΔDD_{ARF} following nomenclatures described in section 2. There are 5 adjustable parameters in the model: E, $^{HD}KIE_c$, $^{HD}KIE_h$, γ_c, γ_h. We optimize these parameters to fit the isotopic and H_2 abundance data obtained from the three sets of experiments (Table S1). All but one parameter are identical across these experiments, except for the efficiency (E) of experiment B, which we allow to be lower as a result of reduced H_2 headspace pressure.

Parameter	Best fit	
	Exp. A and C	Exp. B
E	0.6	0.35
$^{HD}KIE_c$	1.07	1.07
γ_c	1.045	1.045
$^{HD}KIE_h$	1.09	1.09
γ_h	0.97	0.97

Table S1. Best fit parameters for the isotopic model of hydrogenotrophic methanogenesis.

APPENDIX REFERENCES

Horita J. and Wesolowski D. J. (1994) Liquid-vapor fractionation of oxygen and hydrogen isotopes of water from the freezing to the critical temperature. *Geochim. Cosmochim. Acta* **58**, 3425–3437.
Jones W. J., Paynter M. J. B. and Gupta R. (1983) Characterization of *Methanococcus maripaludis* sp. nov., a new methanogen isolated from salt marsh sediment. *Arch. Microbiol.* **135**, 91–97.
Suess H. E. (1949) Das Gleichgewicht H_2 + HDO HD + H_2O und die weiteren Austauschgleichgewichte im System H_2, D_2 und H_2O. *Zeitschrift für Naturforsch. - Sect. A J. Phys. Sci.* 4, 328–332.
Wang D. T., Welander P. V. and Ono S. (2016) Fractionation of the methane isotopologues $^{13}CH_4$, $^{12}CH_3D$, and $^{13}CH_3D$ during aerobic oxidation of methane by *Methylococcus capsulatus* (Bath). *Geochim. Cosmochim. Acta* **192**, 186–202.
Whitehill A. R., Joelsson L. M. T., Schmidt J. A., Wang D. T., Johnson M. S. and Ono S. (2017) Clumped isotope effects during OH and Cl oxidation of methane. *Geochim. Cosmochim. Acta* **196**, 307–325.

Declaration of interests

☐The authors declare that they have no known competing financial interests or personal relationships that could have appeared to influence the work reported in this paper.

☒The authors declare the following financial interests/personal relationships which may be considered as potential competing interests:

Xavier MANGENOT reports financial support was provided by TotalEnergies OneTech. Xavier Mangenot reports a relationship with TotalEnergies OneTech that includes: funding grants.

HIGHLIGHTS.

- First clumped isotope measurements on natural H_2 samples
- Method improved to correct for instrument baselines and non-linearity issues
- ΔDD generally records temperatures of fluid venting or long-term storage
- Cultured hydrogenotrophic methanogens drive the ΔDD value of residual H_2 toward equilibrium at environmental temperatures

Figure 1

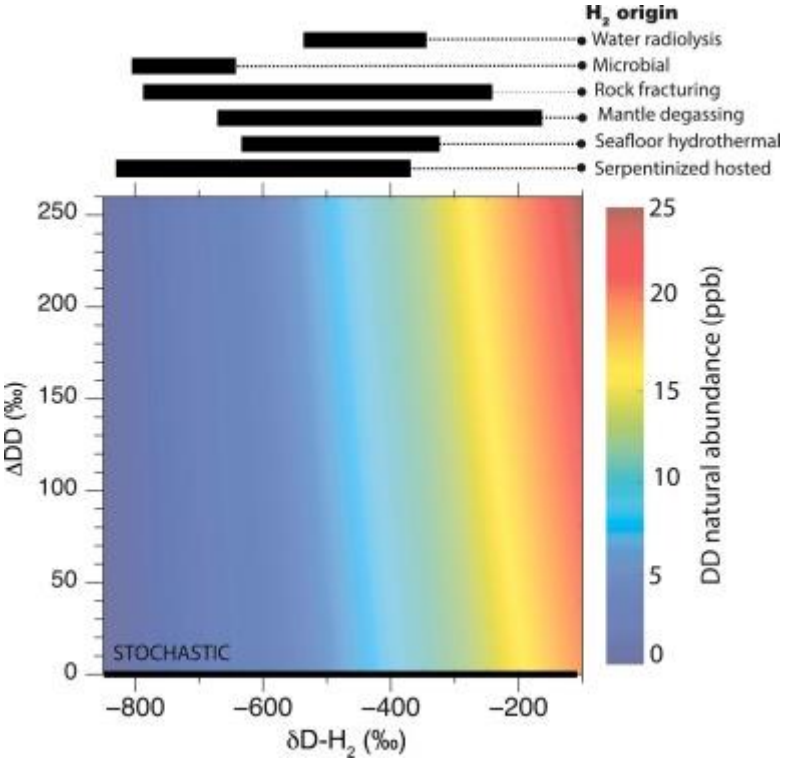

Figure 2

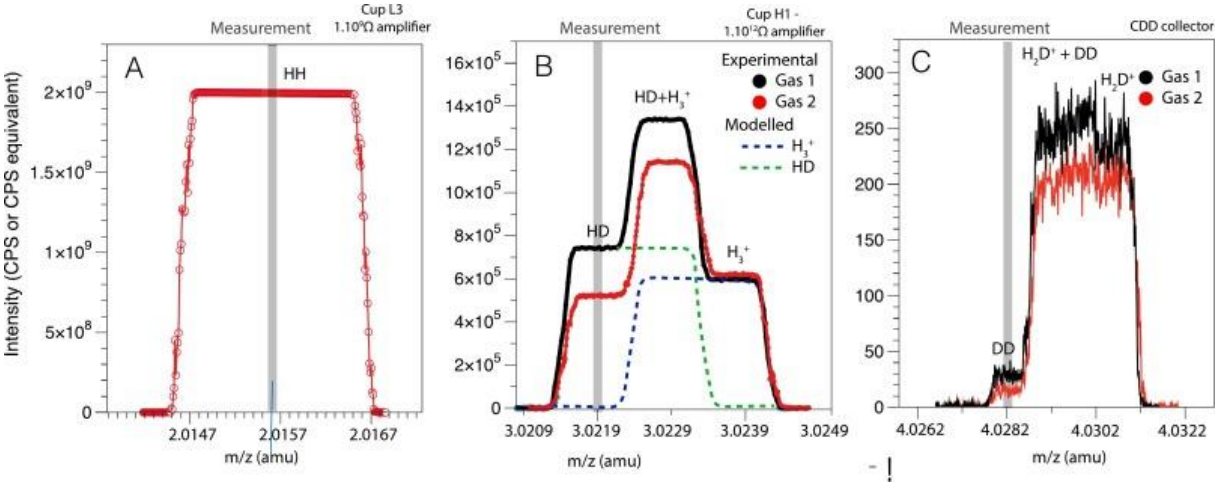

Figure 3

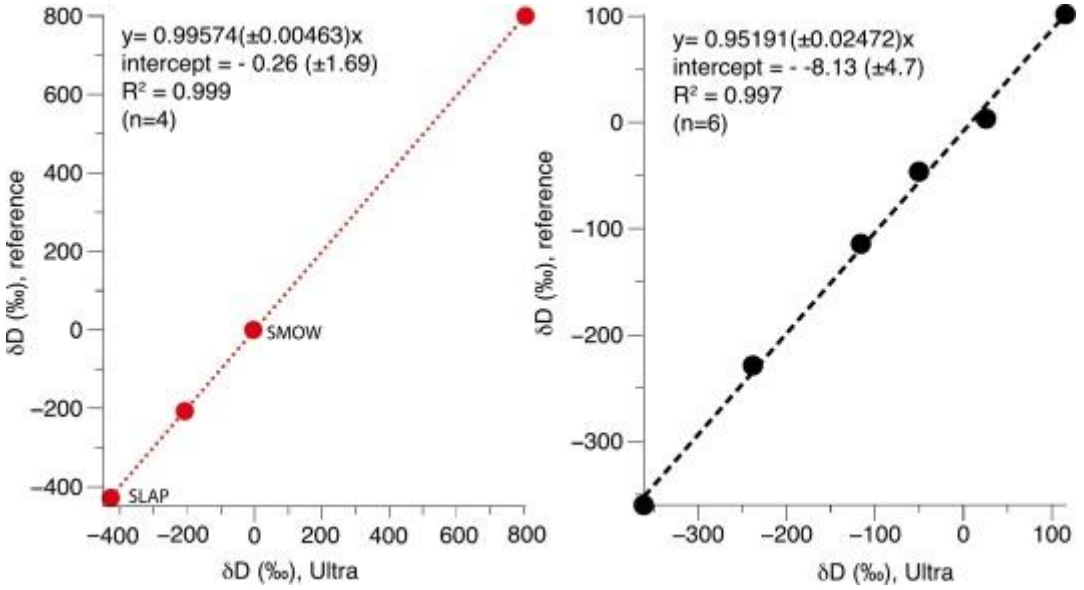

Figure 4

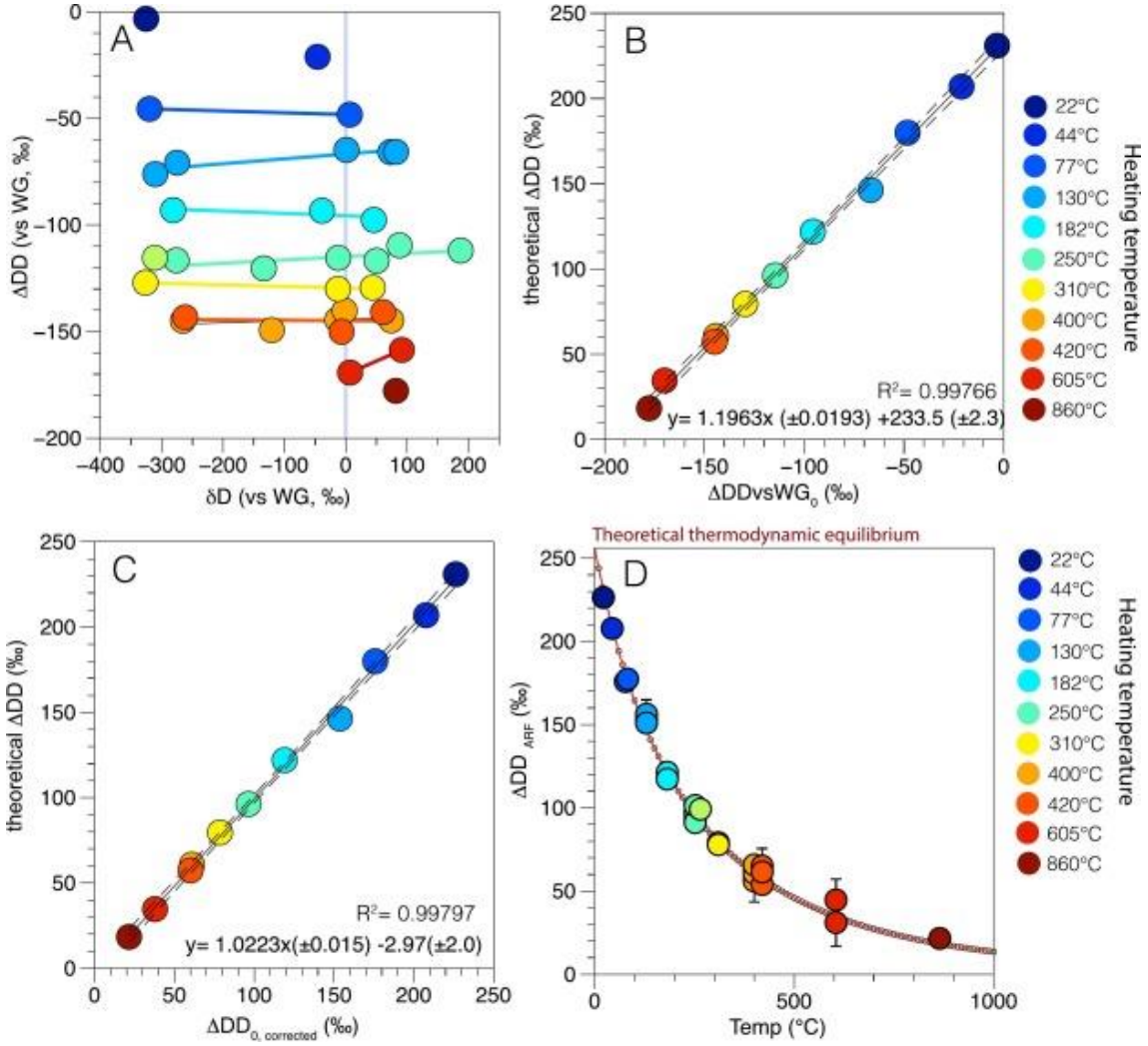

Figure 5

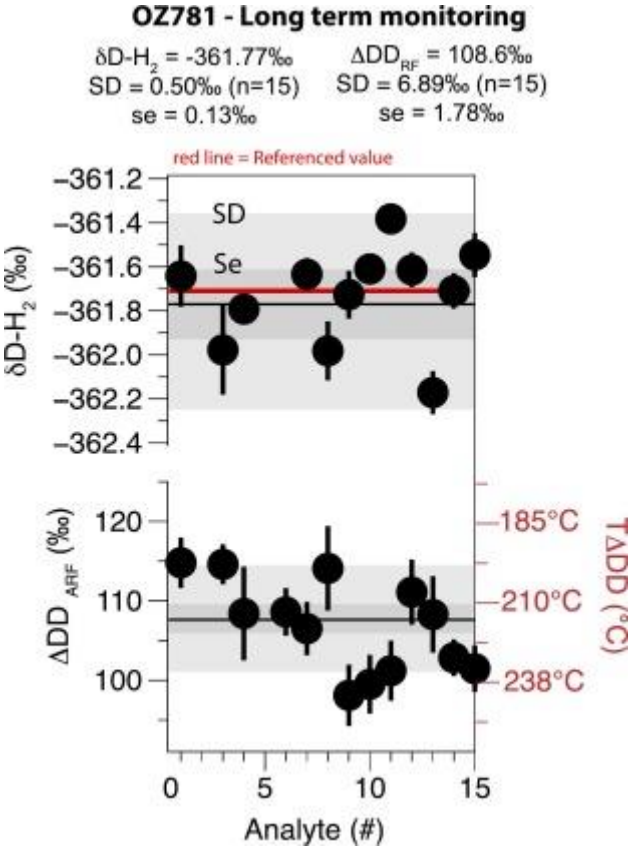

Figure 6

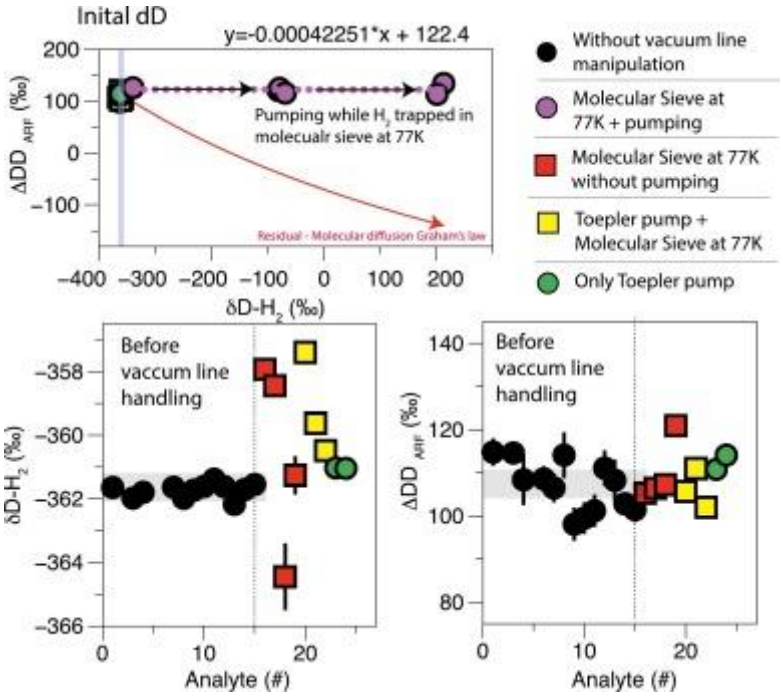

Figure 7

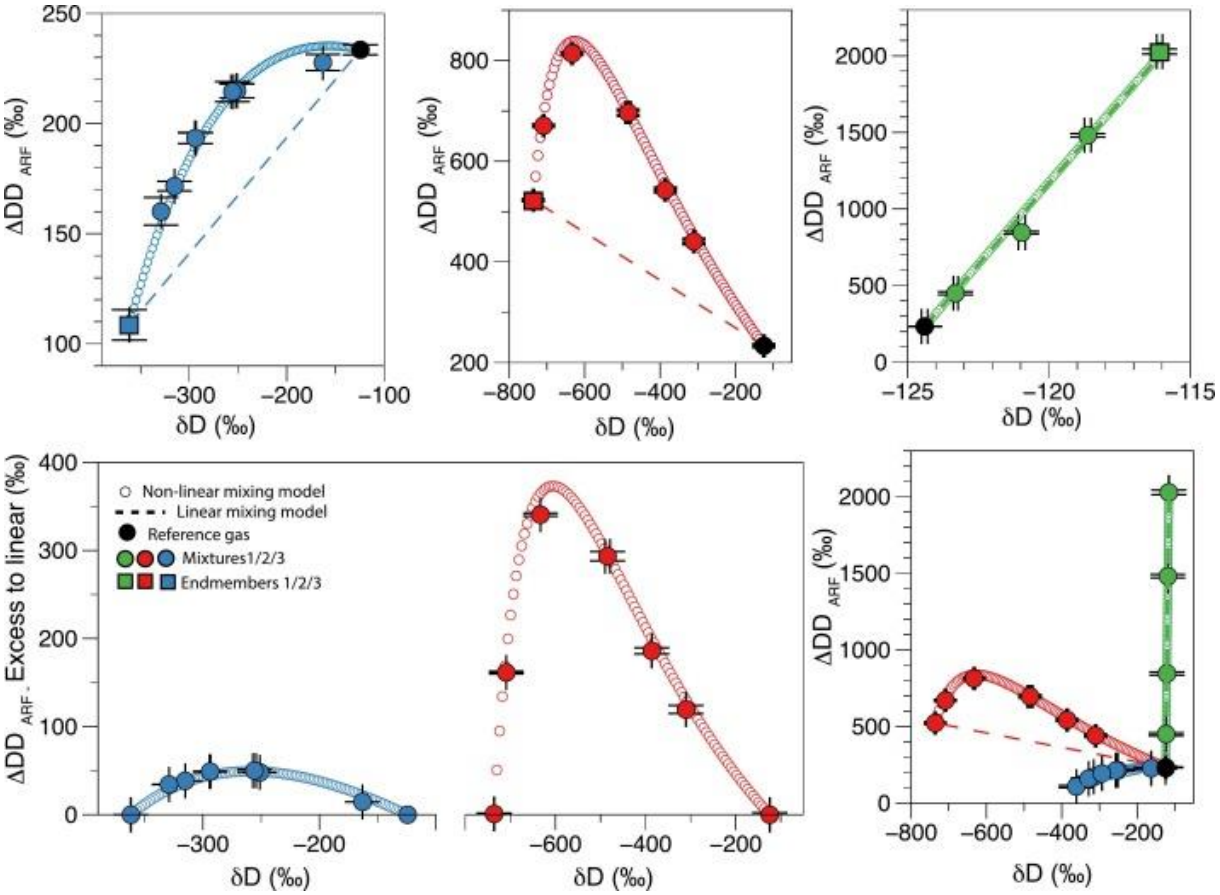

Figure 8

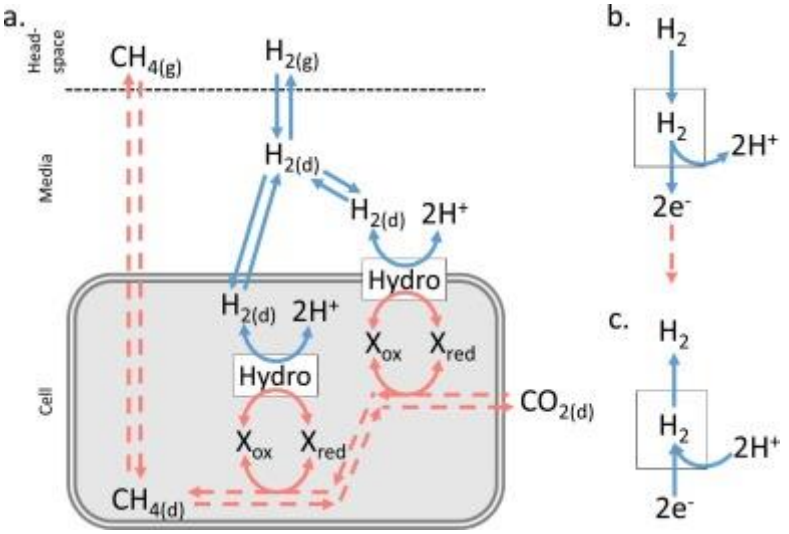

Figure 9

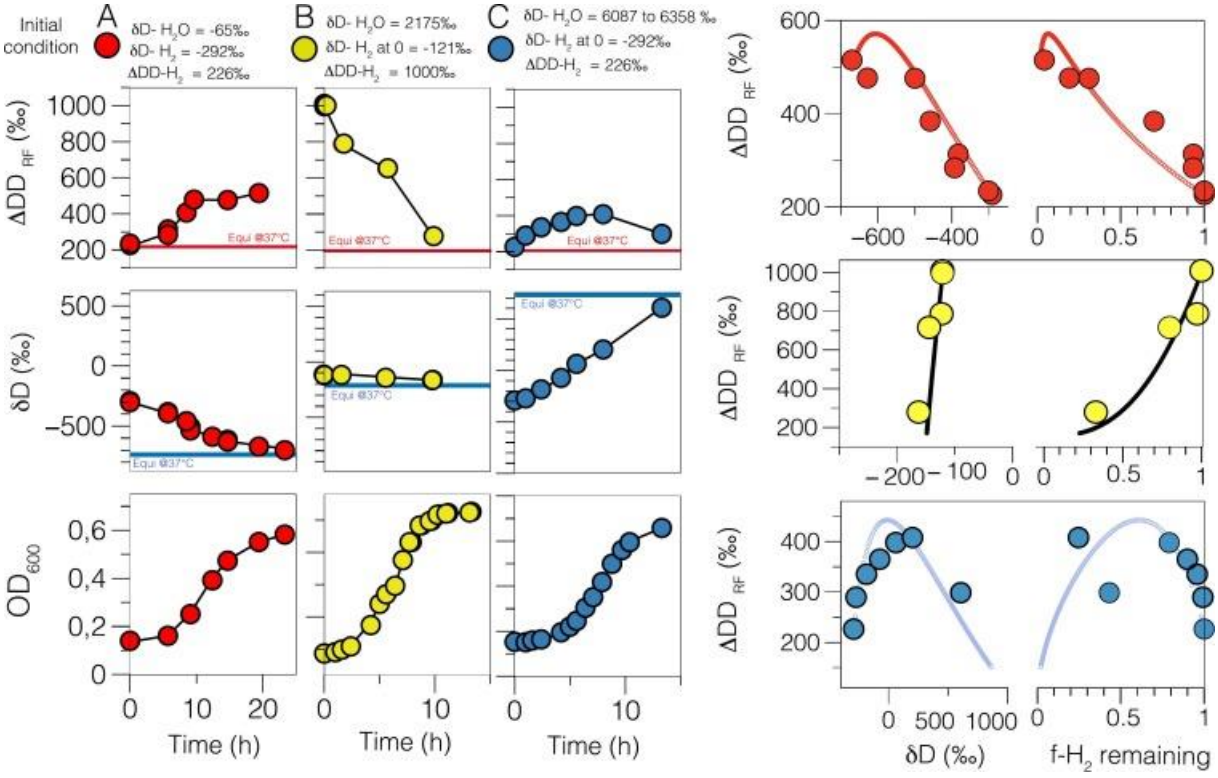

Figure 10